Title
Ignition and spread of electrical wire fires

Author
Huang, Xinyan

Publication Date
2012

Peer reviewed|Thesis/dissertation

UNIVERSITY OF CALIFORNIA, SAN DIEGO

Ignition and Spread of Electrical Wire Fires

A thesis submitted in partial satisfaction of the
requirements for the degree
Master of Science

in

Engineering Sciences (Mechanical Engineering)

by

Xinyan Huang

Committee in charge:

Professor Forman A. Williams, Chair
Professor Kalyanasundaram Seshadri
Professor Carlos F. Coimbra

2012

The thesis of Xinyan Huang is approved, and it is acceptable in quality and form for publication on microfilm and electronically:

Chair

University of California, San Diego

2012

DEDICATION

To Ru-Ting
Love of my life and my soulmate

EPIGRAPH

old country waning moon
sinking in a deep pond
heavy as those stones
words you lay into history
let the course of the river bend

how many blossoms
drive the rise and fall of dynasties
the crows are the drumbeats
emperors like silkworms spin
weaving a long scroll for you

the legendary beauties like clouds
escort the voyages in the heart
a green lamp lifts a corner of the dream
you curl into a flame
that turn into heavy snow

holding wine in the wind
aging with China
a long corridor cuts through springs and autumns
strangers at the gate
are pounding on the knocker

"THE GREEN LAMP"
by Bei Dao

TABLE OF CONTENTS

LIST OF FIGURES

LIST OF TABLES

NOMENCLATURE

Symbols

A	cross-sectional area, mm^2
B	mass-transfer number
Bi	Biot number
c	specific heat, kJ/kg K
c_D	descending velocity, mm/s
d	diameter, mm
H	enthalpy of wire core, $\int_0^\infty \int_{T_a}^{T(x)} A_c \rho_c c_c dT dx$, J
ΔH_c	heat released in combustion of the polymer per unit mass, kJ/kg
h	heat-transfer coefficient, W/m^2 K
h_b	boiling heat-transfer coefficient, W/m^2 K
l	region length, mm
L	heating length, mm
L_p	pyrolysis heat of polymer, kJ/kg
$\dot{m}''$	mass-loss rate per unit area, mg/s mm^2
Nu	Nusselt number
P	perimeter, mm
P_a	atmospheric pressure, atm
P_{O_2}	oxygen partial pressure, kPa
$\dot{q}_e''$	external heat flux to wire, kW/m^2
$\dot{q}_f''$	heat flux from the flame, kW/m^2
$\dot{q}_{loss}''$	heat loss in the heating zone, kW/m^2
$\dot{q}_R'$	heat transfer rate per unit length in the radial direction, kW/m
ΔQ	additional heat in transition, J
R	resistance to flame spread, kJ/m
t	time, s
Δt	additional heat duration, s
T	temperature, K

ΔT	temperature change, K
T_f	flame temperature, K
V_f	flame-spread rate, mm/s
W_f	flame width, mm
x	distance along the wire, mm
X_{O_2}	oxygen concentration, %
$Y_{Q_2,\infty}$	ambient mass fraction of oxygen

Greek

α	thermal diffusivity, m^2/s
γ	curvature augmentation coefficient
δ	characteristic length/thickness, mm
η	heating efficiency from flame
λ	thermal conductivity, kW/m K
ξ	dripping factor
ρ	density, kg/m^3
σ	Stefan-Boltzman constant
ϕ	stoichiometric air-fuel mass ratio

Subscripts

a	ambient
c	metal core
crt	critical condition
$cond/conv$	conduction/convection
ig	ignition
max	maximum
o	outer surface
p	polymer insulation
0	at $x = 0$
1,2,3,4	Regions I, II, III, and IV
$+/-$	right/left-hand side of the interface

ACKNOWLEDGEMENTS

First and foremost I want to thank my advisor Prof. Forman Williams. It has been a great fortune and an honor in my life to be his student. He has taught me, both consciously and unconsciously, how beautiful and exciting combustion science is. I appreciate all his contributions of time, ideas, and guidance to make my academic experience productive and stimulating. He patiently taught me, not only on various aspects of combustion theory, but also the right attitude in which to conduct research and toward life. The joy, humility and devotion he has for his research was deeply contagious and motivational for me to become an outstanding scientist in my future academic career.

I would like to express my gratitude to Dr. Michael Gollner, who is like a big brother to me and always makes time for me from his busy schedule. When I first came to UCSD, I knew little about combustion and fire. He first introduced me to fire research and tutored me in conducting fire experiments. I had a really unforgettable time working with him in the lab and discussing ideas with him in front of the white board. I appreciate his help for reading my papers and correcting my English every time. I am especially grateful for his enthusiasm, friendship, and all the efforts to introduce me to the Ph.D. program at Imperial College, London.

I very much appreciate Prof. Yuji Nakamura for providing with me such a wonderful opportunity to perform all the experiments I needed to complete in this thesis at Hokkaido University, Japan. His patience and preciseness has helped me to gain a deeper understanding of fire science. I appreciate his understanding as well as the time for discussions during many difficult times in my research.

I also wish to thank Prof. Kalyanasundaram Seshadri and Carlos Coimbra for serving on my defense committees, as well as Prof. Yousef Bahadori, Juan Lasheras and Keiko Nomura for offering me TA positions. It has been a great experience to study and work with them. For this thesis, I want to thank Gao Jian, Junya Iwakami, and Yangkyun Kim at Hokkaido University. I appreciate the time they spent with me to discuss this research and their help for my experiment.

I have met many good friends here at UCSD. It is hard to acknowledge all of them here. Some of them are Tran Nguyen, Ryan Gehmlich, Ulrich Niemann,

Wang Longhao, Zhang Shun, and Shen Xie. Their support and sharing parts of their lives kept with me has me grounded and helped me grow. I own special thanks to my old friends, Hao Menglong (Purdue Univ.), Gong Guangjie (Southeast Univ.), Xiang Yixiong (Singapore) and Tao Yang (Qinghua Univ.). Despite thousands of miles of distance between us, I am forever grateful for their phone calls, time and trust.

I thank my parents for creating the best possible learning environment for me over the years. With their support, I feel extremely priviledge to be able to fully devote myself to this intellectual venture.

Over the past year, I have been deeply grateful for the love that Ru-Ting has brought to me. Her smile and encouragement enabled me to be best of myself and go through all the tough times in graduate school. This thesis is dedicated to her.

Xinyan Huang
La Jolla, California
May 14, 2012.

VITA

2010	B. S. in Thermal Energy and Power Engineering, Southeast University, Nanjing, China
2012	M. S. in Mechanical Engineering, University of California, San Diego

PUBLICATIONS

Huang, X., Nakamura, Y., and Williams, F. A., Ignition-to-Spread Transition of Externally Heated Electrical Wire, *Accepted for Publication*, 34^{th} *Proceedings of the Combustion Institute*.

Gollner, M. J., **Huang, X.**, Cobian, J., Rangwala, A. S. and Williams, F. A., Upward Flame Spread and Burning of an Inclined Fuel Surface, *Accepted for Publication*, 34^{th} *Proceedings of the Combustion Institute*.

Huang, X., Nakamura, Y., and Williams, F. A., An Experimental Study of Flame Spread over Electrical Wire in Oxygen-Enriched Atmospheres, *Western States Section of the Combustion Institute, Spring Technical Meeting*, Tempe, AZ, March 2012.

Gollner, M. J., **Huang, X.**, Cobian, J., Rangwala, A. S. and Williams, F. A., Burning of Inclined Fuel Surfaces, Western States Section of the Combustion Institute, Spring Technical Meeting, Tempe, AZ, March 2012.

Huang, X., Nakamura, Y., and Williams, F. A., An Experimental Study on Ignition of Electrical Wire, Western States Section of the Combustion Institute, Fall Technical Meeting, Riverside, CA, October 2011.

Gollner, M. J., **Huang, X.**, Rangwala, A. S. and Williams, F. A., Effects of Inclination on Upward Flame Spread, Western States Section of the Combustion Institute, Fall Technical Meeting, Riverside, CA, October 2011.

Gollner, M. J., **Huang, X.**, Williams, F. A. and Rangwala, A. S., Buoyancy-enhanced flame spread over continuous surfaces, Seventh U.S. National Meeting of the Combustion Institute, Atlanta, GA, March 2011.

FIELDS OF STUDY

Major Field: **Mechanical Engineering**

Studies in Combustion Science
Professors Forman A. Williams and Kalyanasundaram Seshadri

Studies in Fluid Mechanics
Professors Daniel Tartakovsky, Eric Lauga and Alison L. Marsden

Studies in Applied Mathematics
Professors Forman A. Williams and William R. Young

ABSTRACT OF THE THESIS

Ignition and Spread of Electrical Wire Fires

by

Xinyan Huang

Master of Science in Engineering Sciences (Mechanical Engineering)

University of California, San Diego, 2012

Professor Forman A. Williams, Chair

Ignition of electrical wires by external heating is investigated in order to gain a better understanding of the initiation of electrical-wire fires. An ignition-to-spread model is developed to systematically explain ignition and the following transition to spread. The model predicts that for a higher-conductance wire it is more difficult to achieve ignition and the weak flame may extinguish during the transition phase because of a large conductive heat loss along the wire core. Wires with two metal-core materials, nichrome and copper having three different diameters, with polyethylene coatings of three different thicknesses are employed and a coil heater was adopted as the ignition source in the experimental study. Experiments show that additional heating times after flash are required in order to fully pass the transition and achieve a spreading flame, agreeing with model

predictions. In addition, the effects of different heating lengths, ambient pressures and oxygen concentrations on wire ignition are discussed.

Steady flame spread horizontally along thin electrical wires in normal and oxygen-enriched oxygen/nitrogen atmospheres is also investigated both theoretically and experimentally to gain a better understanding of the development of in electrical fires occurring in normal and modified environments. A simplified flame-spread model is developed in an effort to identify the most important effects of the wire thermal conductivity and diameter, the thickness of the insulation, and the oxygen concentration. The experimental results agree qualitatively with the model predictions in a number of respects, while no qualitative disagreements were found. This study may be useful for upgrading the design and standards of future fire-safe wires.

Chapter 1

Introduction

1.1 Electrical Wire Fires

Over the course of a typical year, residential electrical fires account for 28,600 incidents and $1.1 billion in property losses, 53% of which involve electrical wiring [1]. Electrical wire fires are also responsible for nearly 42% of the total number of fire cases in nuclear power plants (NPP) [2]. Most electrical fires are caused by arcing, short circuits, overheating or ground faults, leading to ignition of combustible insulation on attached or nearby wires. These fires may propagate along flammable insulation to different rooms and floors, and they may ignite other nearby combustibles, increasing fire damage (Fig. 1.1).

Electrical wire faults are also a probable fire scenario in sub-atmospheric pressure and microgravity applications, such as aircraft and space vehicles [3–5]. Once ignited, with a weak flow for the purpose of ventilation fires may continue to propagate along flammable insulation of power or control wires and other nearby combustibles, generating heat, smoke and toxic gases, leading to extensive damage. For example, arc-initiated fire from a harness was responsible for the Swiss air accident in 1998 [6]. In these reduced-pressure environments, the oxygen percentage is often increased to sustain a normal oxygen partial pressure (21 kPa), to support adequate human performance and to minimize side effects on human health, while creating a more flammable atmosphere. Therefore, there is also a motivation to investigate of how wire fires develop in oxygen-enriched atmospheres.

Figure 1.1: (a) Airplane fires; (b) Nuclear power plant fires; (c) Chemical plant fires; (d) Electrical fires.

1.2 Literature Review

Various standards and tests have been developed to evaluate the fire performance of electrical wires [7]. For example, Fernandez-Pello et al. [8] investigated the ignition and spread characteristics of several complex wires and ranked their fire performance, employing a simple analysis developed by Quintiere et al. [9]. Leung et al. [10] simulated the effect of core-wire conduction on thermal pyrolysis of the insulation layer without flaming during the heating process. Kashiwagi [11–13] systematically investigated how the radiation and oxygen concentration affected the ignition properties of polymer materials, the result of which showed that the gasification rate increased with the oxygen concentration and radiation was absorbed within the 1-2 mm polymer layer. Umemura et al. [14] proposed a numerical model to solve the initial phase of electrical wire ignition and spread in microgravity. Fujita et al. [15] discovered that ignition of electrical wire insulation with short-term excess electrical current was easier to obtain in microgravity than under normal

gravity.

Bakhman et al. [16, 17] performed extensive experiments to investigate the flame spread and critical burning conditions for polymethylmethacrylate (PMMA) and polyethylene (PE) insulation on copper wires. The results demonstrated that the flame-spread rate increased with decreasing coating thickness in all upward-spread, horizontal-spread, and downward-spread configurations, and heat conduction through the wire core enhanced the burning rate. Delichatsios et al. [18] developed semianalytical expressions for creeping flame spread over thin fuel cylinder by Oseen approximation, the result of with agreed well with numerical and experimental results. Tewarson and Khan [19] reported that the rates of flame spread over laboratory-scale wire samples in oxygen enriched atmosphere are comparable to the rate in larger-scale wire fires, but recently Beaulieu [20] emphasized that the accuracy of simulation large-scale flame heat flux by oxygen-enriched test depended on test orientations. Fujita and co-workers [21, 22] carried out experimental studies on downward flame spread along thin wires at both microgravity and normal-gravity condictions in oxygen-enriched environments (mole fractions $X_{O_2} = 30\% \sim 50\%$) with different diluent gases, observing that the spread rate increased as the wire diameter decreased, while the ambient pressures had relatively little effect. Kim et al. [23] performed a numerical study on the molten process of phase change material (PCM) to understand how the material properties affect molten and dripping condition of polymer under a localized thermal input.

Previous studies have demonstrated that the flame-spread rate over insulated electrical wires increases with decreasing pressure and increasing wire conductivity, resulting in a higher likelihood of fire propagation [24, 25]. Two distinctive modes, flame-driven and wire-driven, were found to control wire fire-spread behavior, and both modes are affected by the conductance (e.g. thermal conductivity and diameter) of the wire core. During the flame-spread experiments, it was also found that in low-pressure environments achieving wire ignition by an external heating source was more difficult, exemplifying the difference between ignition and flame-spread phenomena over wires [26].

1.3 Outline of the Thesis

Although several previous studies have focused on either ignition or spread separately, to the authors' best knowledge, no study has systematically addressed the transition from ignition to spread or how both the dimension and the thermal conductance of the wire, as well as the oxygen concentration affect the flame-spread rate. This study first develops a simplified ignition model to predict ignition and the subsequent transition to flame spread over electrical wires. Then, a simplified model is developed to predict the burning rate and the spread rate of wire fires for different wires and under different ambient conditions.

In order to test these models, experimental studies on ignition and flame-spread are performed with several thin wires for various oxygen concentrations and pressures. The influence of wire configuration, heating conditions and ambient environment on the ease of ignition and the rate of flame spread are investigated. The results of this study may provide a first step towards acquiring information that is useful in establishing fire-safety standards for widely used electrical wires and other multilayer materials.

Chapter 2

Theory

2.1 Ignition Model

2.1.1 Flashpoint

Assume that there is a long wire, the partial length (L), exposed to an external heat flux, $\dot{q}_e''$ (convection, radiation, or combined) for a finite period (t_h). Because of the symmetry of the wire and heating zone, only half of the wire is considered, with an adiabatic boundary condition at the heated center (Fig. 2.1a). The flashpoint is usually defined as the minimum condition under which pyrolysis vapors achieve a fuel's lower flammability limit [27], denoted by either a critical surface temperature or a critical fuel mass flux [9]. In this model, a constant ignition temperature (T_{ig}), which is a few degrees higher than the pyrolysis temperature of the polymer coating, is selected. With a pilot source, the first flash will be achieved once the maximum temperature in the wire reaches T_{ig} (Fig. 2.1b).

In order to simplify the system, we assume (1) a perfect thermal contact between the central wire core and the insulation coating, (2) materials that are isotropic, and (3) no thermal expansion or deformation occurs during heating. The polymer coating in this study is thermally thin (thickness $\delta_p \sim 0.2$ mm $\ll \sqrt{\alpha_p t_h}$ with $t_h > 3$ s), and its thermal conductivity and thermal inertia are much less than those of the metal core ($\lambda_p \ll \lambda_c$, $(\rho c \lambda)_p \ll (\rho c \lambda)_c$). Therefore, a uniform temperature throughout the cross-section is assumed (Biot Num-

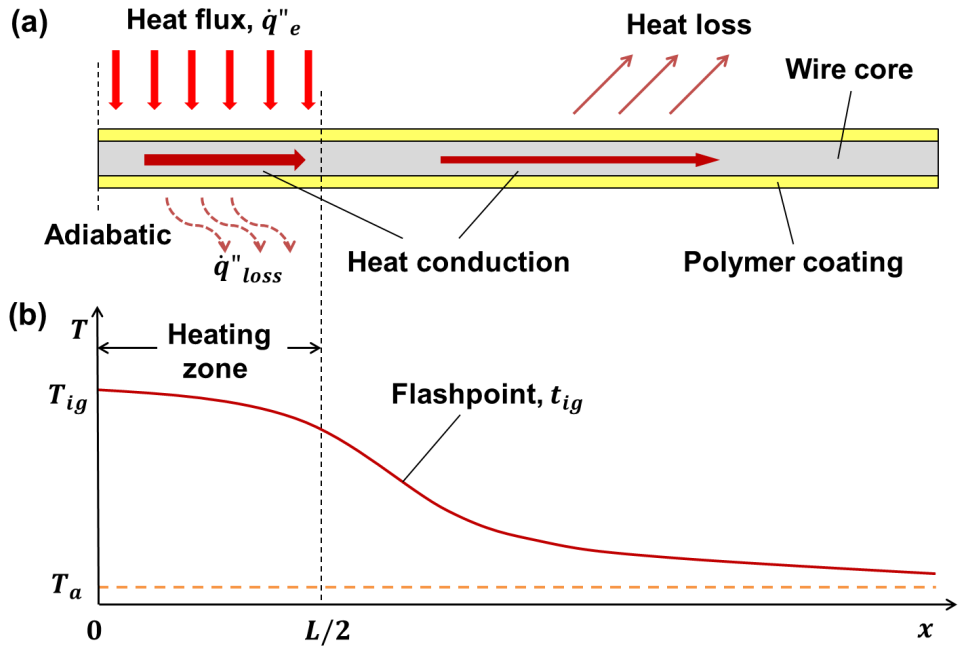

Figure 2.1: Heat-transfer model before ignition: (a) schematic illustration; (b) temperature distribution along the wire core.

ber $Bi_c = hd_c/\lambda_c \ll Bi_p = h\delta_p/\lambda_p < 0.03$), establishing a one dimensional (1-D) heat-transfer model

$$
\begin{aligned}
&(\sum \rho cA)\frac{\partial T}{\partial t} = A_c\lambda_c\frac{\partial^2 T}{\partial x^2} + P_o\left(\dot{q}''_e - \dot{q}''_{loss}\right) \quad (0 < x < \frac{L}{2}) \\
&(\sum \rho cA)\frac{\partial T}{\partial t} = A_c\lambda_c\frac{\partial^2 T}{\partial x^2} - P_o h(T - T_a) \quad (x > \frac{L}{2}) \\
&\text{where} \quad T_{L/2^-} = T_{L/2^+}, \quad \left(\frac{\partial T}{\partial x}\right)_{L/2^-} = \left(\frac{\partial T}{\partial x}\right)_{L/2^+}, \\
&\left(\frac{\partial T}{\partial x}\right)_0 = 0, \quad \text{and} \quad T_\infty = T_a, \quad \text{for} \quad t > 0,
\end{aligned}
\tag{2.1}
$$

and $\sum \rho cA = (\rho cA)_c + (\rho cA)_p$. Here, d, A, ρ, c, and λ are the diameter, cross-section area, density, heat capacity, and thermal conductivity, respectively, with the subscript c for core metal and p for polymer coating; P_o is the outer perimeter, $\dot{q}''_{loss}$ is the heat flux from the wire surface in the heating zone, T_a is the ambient temperature, and h is the heat-transfer coefficient outside the heating zone. The temperature dependences of all parameters are accounted for in the calculation. With the initial condition $T(t = 0) = T_a$, Eq. (2.1) can be solved numerically.

When the maximum temperature of the wire core reaches T_{ig}, flash occurs and the heating duration is denoted as an ignition time ($t_{ig} = t_h$) whose functional dependence is expressed by an empirical equation as [28]

$$t_{ig} \approx \frac{f(\lambda, d_c, \delta_p, L)}{\dot{q}_e''^n}, \tag{2.2}$$

where the index n denotes an ignition property of the fuel, determined by the configuration of the wire and the heating conditions. Ideally, for a thermally thin fuel $n \approx 1$, and $n \approx 2$ for a thermally thick fuel [28].

As the external heat flux decreases, a longer heating time is required, and the temperature profile at the flashpoint in Fig. 2.1b will be broader. Upon reducing the heat flux, the wire may reach thermal equilibrium with its surroundings before reaching its ignition temperature. Then, a critical or minimum ignition heat flux, $\dot{q}''_{e,crt}$ can be calculated by neglecting the time dependence in Eq. (2.1), $\partial T/\partial t = 0$. When the temperature variation within the heating zone is small ($T_{L/2} \approx T_{ig}$), the critical heat flux becomes

$$\dot{q}''_{e,crt} = \dot{q}''_{loss} + \frac{P_o}{L}(T_{ig} - T_a)\sqrt{h\lambda_c d_o}. \tag{2.3}$$

The second term on the right side represents the steady-state conduction through wire core, derived from Eq. (2.1). Clearly, with a short heating length L or a large conductive heat loss from the wire core, the critical heat flux increases and ignition becomes difficult. As the heating length increases, the critical heat flux will approach $\dot{q}''_{loss}$ and it becomes less dependent on the wire conductance.

2.1.2 Spread Point

To help describe the ignition-to-spread transition, the temperature distribution during steady-state flame spread is considered. As shown in Fig. 2.2, the coordinate system is fixed to the location of the flame, and the wire moves at a velocity $-V_f$. In the steady state [25], the heat-transfer equation within the wire core becomes

$$A_c\lambda_c\frac{d^2T}{dx^2} + V_f\left(\rho_c c_c A_c\right)\frac{dT}{dx} = \dot{q}'_R, \tag{2.4}$$

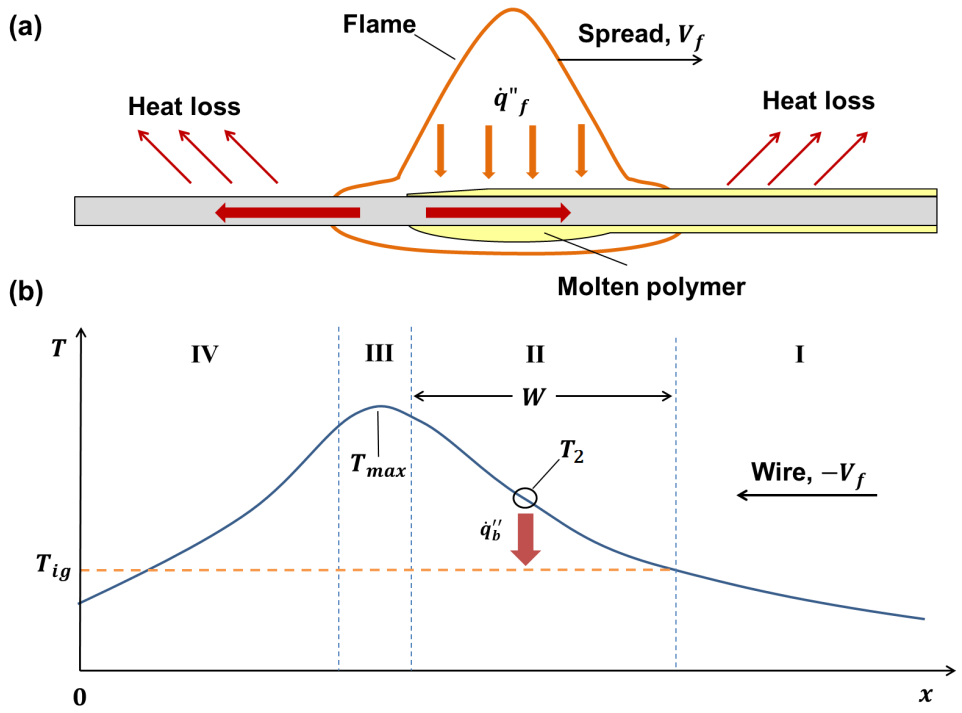

Figure 2.2: Heat-transfer model in steady-state spread: (a) schematic illustration; (b) temperature distribution along the wire core.

where $\dot{q}'_R$ is the heat transfer rate per unit length in the radial direction. In general, there are four regions in the wire with different boundary conditions: (1) unburned wire with a polymer coating where $\dot{q}'_R = P_o h(T - T_a)$ and $\sum \rho c A$ instead of $\rho_c c_c A_c$ is considered; (2) a boiling polymer within the flame zone; (3) an exposed wire core within the flame zone; and (4) a wire core exposed to the ambient atmosphere where $\dot{q}'_R = P_c h(T - T_a)$. The flame structure will be further discussed in next chapter. In this ignition model, only the temperature profile during the spread is considered.

In Region (2), the wire core's temperature is higher than the ignition temperature, so that it acts as an additional source to heat the polymer coating. By neglecting the complex shape and surface-tension effects of the molten polymer [10], regions (2) and (I2) are simplified to a point heat source with an average temperature of $T_2 \approx (T_{max} + T_{ig})/2$, which heats the molten polymer through boiling heat transfer, $\dot{q}''_b \approx h_b(T_2 - T_{ig})$ where $h_b \sim \lambda_p/\delta_p$ is the boiling heat transfer coefficient. With experimental measurements of the steady flame-spread rate, V_f

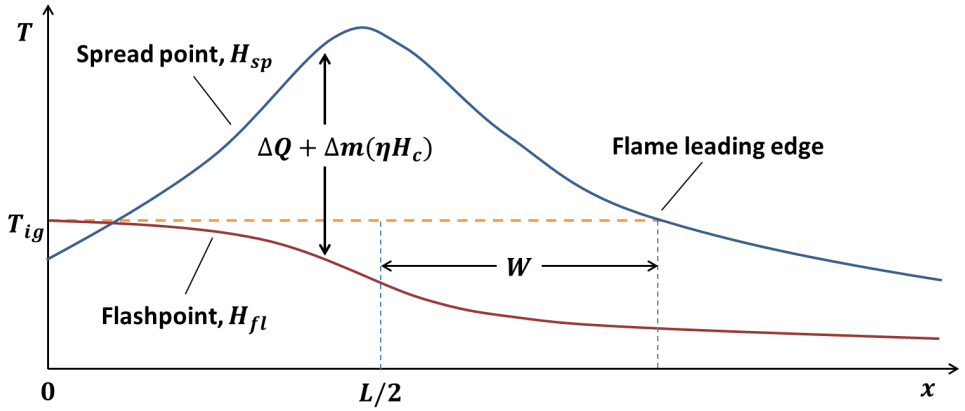

Figure 2.3: Temperature profile of ignition-to-spread transition.

and flame width, W_f, the averaged mass-loss rate per unit area, $\overline{\dot{m}''}$ for a cylinder is [28–30]

$$\begin{aligned} \overline{\dot{m}''} &= \frac{\delta_p \rho_p}{W_f} V_f \approx \frac{Nu \cdot \lambda_g}{c_g d_o} \ln(1+B), \\ \text{where} \quad B &= \frac{Y_{O_2,\infty}(\Delta H_c/\phi) + c_g(T_a - T_{ig})}{L_p - \dot{q}_b''/\overline{\dot{m}''}}, \end{aligned} \tag{2.5}$$

ΔH and L_p are the combustion and pyrolysis heat of the polymer per unit mass; $Y_{O_2,\infty}$ and ϕ are the ambient oxygen mass fraction and the stoichiometric air-fuel mass ratio, and Nusselt number (Nu$\sim$0.5) is calculated from a numerical solution [31]. The modified mass-transfer number ($B \sim 5$) can be calculated to estimate T_{max} in the wire core. Then, the temperature profile during steady-state spread can be evaluated. For a higher-conductance wire, the flame width is larger and the temperature profile in the wire core is expected to be broader.

2.1.3 Ignition-to-Spread Transition

After the flashpoint, for the flame to spread the unstable flame must be strong enough to bring the temperature profile to that at steady-state spread (Fig. 2.3). However, during this ignition-to-spread transition, large conductive heat losses along the metal core may quench the weak flame and prevent its spread. Therefore, additional heat, ΔQ or an additional heating duration, Δt is needed to continue heating the wire and sustain the weak flame. Here, we define a spread

point, where self-sustained flame spread occurs only if the heat flux from the flame or other external heat sources can bring the temperature profile of the wire core outside the heating zone up to that at steady-state spread. Thus, ΔQ or Δt is determined the by the wire temperature distribution and available fuel in the heating zone, which can be estimated as

$$\begin{aligned} \Delta Q &= (H_{sp} - H_{fl}) - \Delta m(\eta \Delta H_c), \\ \Delta t &= \Delta Q / (\dot{q}_e'' P_o L/2), \end{aligned} \tag{2.6}$$

where $\Delta m = (L/2)\rho_p A_p$ and η are the mass of fuel consumed and the flame heating efficiency, so $\Delta m(\eta \Delta H_c)$ is the heat from flame to the wire core, which depends on the thickness of the polymer coating and the length of the heating zone. The enthalpy of the wire, $H = \int_0^\infty \int_{T_a}^{T(x)} (\sum \rho c A) dT dx$, at the flashpoint ($H_{fl}$) and spread point ($H_{sp}$) can be determined by solving Eq. (2.1) and Eq. (2.4), respectively.

For a high-conductivity wire or a short heating length, the enthalpy gap between the flashpoint and spread point becomes large, and a long additional heating time is expected. For a long heating length or a low-conductivity wire, the heat from the weak flame may be sufficient to bring the temperature profile of the wire above the spread point, in which case no additional heating is needed beyond the flashpoint.

2.2 Flame-Spread Model

Flame spread can be viewed as an ignition process originating from a point of fire inception, where the flame acts as both a pilot and a heating source [32,33]. Once the fuel surface reaches the ignition temperature and the pyrolyzed fuel reaches the critical mass flux, ignition will occur [27]. The ignition temperature is roughly the pyrolysis temperature, $T_{ig} \approx T_p$, which for some polymers (e.g. polyethylene) may decrease with increasing oxygen concentration due to oxidative pyrolysis [12].

In fire spread over thin electrical wires (Fig. 2.4), the large-conductivity metal core ($\lambda_c \gg \lambda_p$) effectively transfers a large amount of heat from the burning

region downstream to the leading edge of the flame where the local flame contributes little and acts primarily as a pilot source. Therefore, heat conduction through the solid phase dominates preheating of the fuel and appreciably increases the fire propagation velocity.

2.2.1 Flame Structure

A simplified description of steady flame spread along a thin electrical wire at a constant velocity of V_f is illustrated in Fig. 2.4. The coordinate system is fixed to the leading edge of the flame ($x = 0$) where the wire moves at a velocity of $-V_f$ in the x direction. Ahead of the spread point, a steady temperature profile along the wire core can be calculated by a heat-transfer equation

$$A_c\lambda_c\frac{d^2T}{dx^2} + (\rho_c c_c A_c)\, V_f \frac{dT}{dx} = \dot{q}_R^{'}. \tag{2.4}$$

Four regions can be identified in the wire with different boundary conditions: (I) unburned wire with a polymer coating; (II) a pyrolyzing polymer within the yellow flame zone; (III) an exposed wire core with a blue flame tail; and (IV) an exposed wire core cooled by the ambient atmosphere. The visible (yellow) flame width in experiments is equal to the length of Region II, $W_f = l_2$. The shape of the temperature profile, shown in Fig. 2.4, is consistent with recent temperature measurements by a fixed thermocouple during flame spread [34].

In this study, the thermal conductivity of the thermally thin ($\delta_p < 0.5$ mm) polymer coating is much less than that of the metal core ($\lambda_p \ll \lambda_c$) while $\rho_p c_p \approx \rho_c c_c$. So in Region I, a uniform temperature throughout the cross section is hypothesized, where $\rho_c c_c A_o$ is adopted instead of $\rho_c c_c A_c$, and radial heat transfer is primarily by convective and radiative cooling, $\dot{q}_{R,1}^{'} = P_o h_1 (T_1 - T_a)$. With boundary conditions $T(x = 0) = T_{ig}$ and $T(x = \infty) = T_a$, Eq. (2.4) yields the conductive heat-loss rate from Region II to I as

$$\begin{aligned} -A_c\lambda_c\left(\frac{dT}{dx}\right)_{0^+} &= (\rho_c c_c A_o)\frac{V_f}{2}\left[1 + \sqrt{1 + \frac{(\lambda_c A_c)}{V_f^2}\frac{P_o h_1}{(\rho_c c_c A_o)^2}}\right](T_{ig} - T_a) \\ &\approx (\rho_c c_c A_o) V_f \left[1 + \frac{(\lambda_c A_c)}{V_f^2}\frac{P_o h_1}{(\rho_c c_c A_o)^2}\right](T_{ig} - T_a). \end{aligned} \tag{2.7}$$

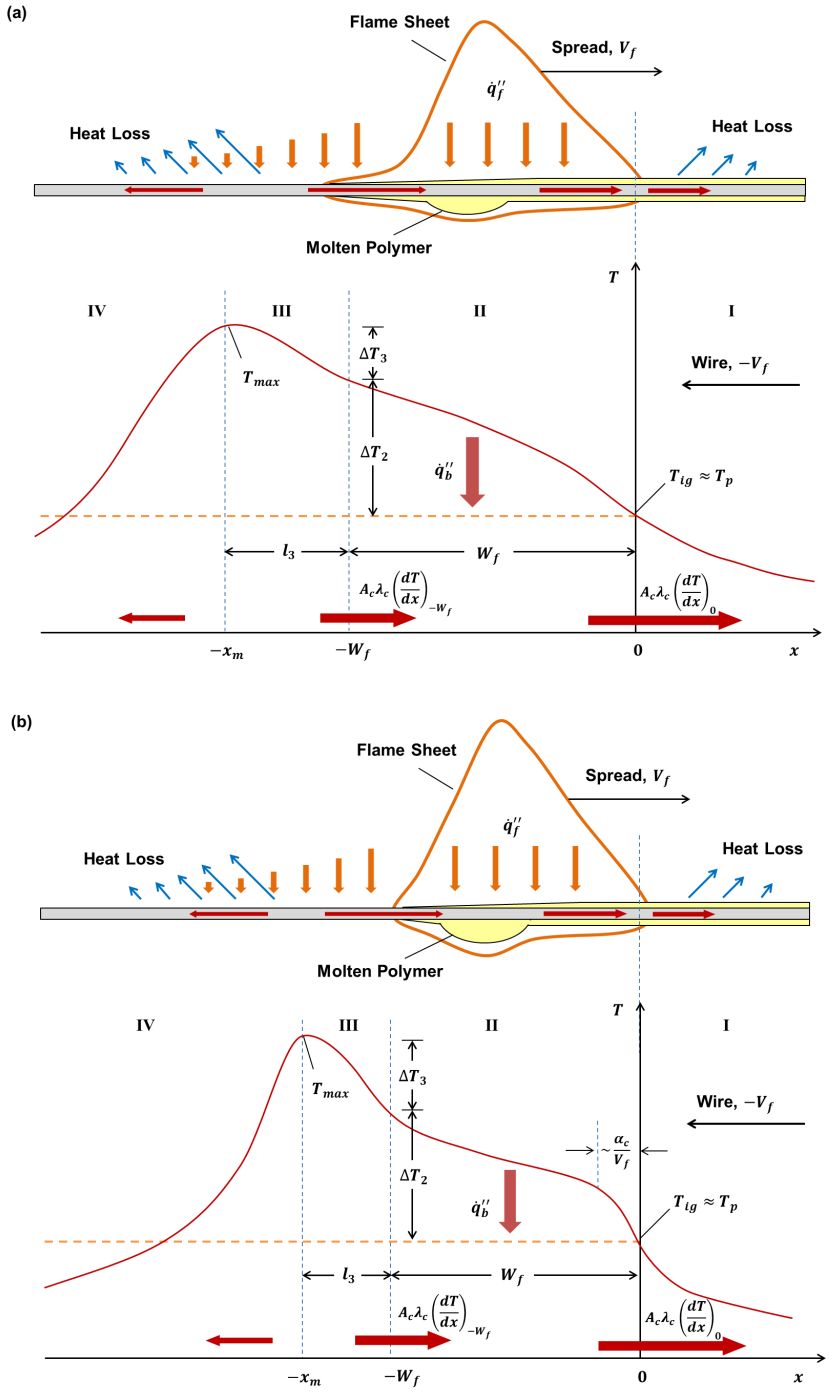

Figure 2.4: Illustration of the flame structure and temperature profile within the wire core during steady-state spread: (a) a high conductivity wire core with a low spread rate ($W_f < \alpha_c/V_f$), and (b) a low-conductivity wire core with a high spread rate ($W_f > \alpha_c/V_f$).

A detailed derivation of the wire-core temperature profile is given in the Appendix. The last approximation in Eq. (2.7) is more accurate for a larger-conductivity core and at a larger spread rate, $4P_o h_1 A_c \lambda_c \ll (\rho_c c_c A_o V_f)^2$. As the spread rate increases, the convection term in Eq. (2.4) becomes increasingly dominant in Region I, stretching the temperature profile and transferring more heat upstream (Fig. A.1). At the same time, the diffusion (conductance) effect becomes small enough to be neglected.

A majority of the molten polymer is pyrolyzed in Region II, and a small molten ball may accumulate at the end. If the polymer coating is relatively thick, not all of the fuel is burned out during flame spread, and dripping of the molten polymer is anticipated and is observed experimentally. The length of Region II is controlled by the burning condition, the residence time of the molten polymer, and the force balance of surface tension with gravity and viscous forces [23], which is difficult to determine analytically. Because the thin molten polymer coating becomes thinner during the pyrolyzing process, only part of the radiation, $(1-\eta)\dot{q}_f''$ from the flame can be absorbed [12], and the rest ($\eta\dot{q}_f''$) penetrates the thin liquid film to directly heat the wire core, bring the temperature higher than the pyrolysis temperature of polymer coating. Here, η will decrease as the coating thickness increases. Thus, the wire core starts to heat the coating through boiling heat transfer, $\dot{q}_b'' = h_b(T - T_{ig})$ where h_b is the boiling heat transfer coefficient which is usually an empirical coefficient that can be correlated with both convective and radiative heat transfer coefficients [35]. In general, h_b is not a constant, which changes with the temperature difference and the liquid viscosity. With $\dot{q}_{R,2}' = P_c[h_b(T - T_{ig}) - (\eta\dot{q}_f'')]$ and the matching conditions at $x = 0$, the temperature change in Region II, $\Delta T_2 = T_{-W_f} - T_{ig}$ can be obtained by solving Eq. (2.4), which decreases with increasing core conductances (Fig. A.2).

In Region III, a weak blue flame is usually observed. The heat flux from the the flame tends to decrease, but continues to heat the wire core mainly through radiation, depending on the total heat flux in Region II and the width and height of the flame roughly as $\dot{q}_f''(x) = \dot{q}_f'' e^{(x+W_f)/W_f}$. It eventually brings the wire core to a maximum temperature at $x = -x_m$ where the heat flux from the flame equals

the surface reradiation and natural convection. Therefore, the length of Region III ($l_3 = x_m - W_f$) can be determined from

$$\dot{q}_f^{''} e^{-l_3/W_f} = \sigma(T_{max}^4 - T_a^4) + h_{conv,3}(T_{max} - T_a), \tag{2.8}$$

which depends on the heat flux from the flame and the temperature of the wire core. If the temperature profile in Region III is shallower, l_3 tends to be longer, and the net heating from the flame to the wire core,

$$P_c l_3 \dot{q}_{f,net}^{''} = P_c \int_{-x_m}^{-W_f} \dot{q}_f^{''} e^{(x+W_f)/W_f} - \sigma[T(x)^4 - T_a^4] dx, \tag{2.9}$$

becomes larger, conducting more heat to pyrolyze the coating in Region II and preheat the unburnt fuel in Region I. For simplicity, a constant net heat flux, $\dot{q}_{R,3}^{'} = P_c \dot{q}_{f,net}^{''}$ is assumed in Region III. With boundary conditions $T_3(x = -x_m) = T_{max}$ and $(dT/dx)_{-x_m} = 0$, solving Eq. (2.4) shows that the heat conduction from Region III to II is

$$-A_c \lambda_c \left(\frac{dT}{dx}\right)_{-W_f} = \frac{\alpha_c P_c \dot{q}_{f,net}^{''}}{V_f} \left(1 - e^{-l_3 V_f/\alpha_c}\right) \approx P_c l_3 \dot{q}_{f,net}^{''} \left(1 - \frac{V_f l_3}{2\alpha_c}\right), \tag{2.10}$$

which is larger for a higher-conductivity wire (Fig. A.3a). The last approximation is valid for $l_3 V_f/\alpha_c < 1$. Also, the temperature change in Region III is

$$\Delta T_3 = T_{max} - T_{-W_f} \approx \frac{P_c l_3^2 \dot{q}_{f,net}^{''}}{\lambda_c A_c}, \tag{2.11}$$

which also decreases with increasing conductance as ΔT_2. Therefore, for a larger-conductance wire, $T_{max} = T_{ig} + \Delta T_2 + T_3$ is smaller, so that both l_3 and $\dot{q}_{f,net}^{''}$ become larger, as shown in Eqs. (2.8) and (2.9).

In Region IV, the heat flux from the flame become negligible and the temperature of the wire core decreases rapidly due to the large heat loss, $\dot{q}_{R,4}^{'} = P_c h_4 (T - T_a)$. During flame spread, few polymer coatings undergo charring and remain on the core, which can be neglected here.

2.2.2 Flame Heat Flux

In Region II, a uniform heat flux from the flame, including both conduction and radiation, is assumed. The conductive heat flux from the flame, $\dot{q}_{f,cond}^{''}$ can be

estimated from an approximate solution of the creeping flame [18, 36]

$$\dot{q}''_{f,cond} = \lambda_g \left(\frac{\partial T}{\partial r}\right)_{r_o} \approx \gamma\lambda_g \frac{T_f - T_{ig}}{\delta_g} \approx \gamma\lambda_g \frac{(B-\phi)L_p}{c_g\delta_g}, \tag{2.12}$$

where γ is the augmentation coefficient because of the cylindrical curvature [18], which is calculated to be about 4 for $d_o \sim 1$ mm and increases slightly with decreasing wire diameter, $\gamma \sim d_o^{\mu}$ with $0 < \mu < 1$. The flame standoff distance, $\delta_g \sim d_o/\mathrm{Nu}$ increases with increasing wire diameter and with decreasing natural convection (e.g. low pressures). Therefore, the heat flux is greater for a thinner wire, $\dot{q}''_{f,cond} \sim d_o^{-(\mu+1)}$ and slightly smaller in reduced-pressure atmospheres. The mass-transfer number B in Eq. (2.12) is [28]

$$B = \frac{Y_{O_2,\infty}(1-\chi_r)\phi\Delta H_c + c_g(T_a - T_{ig})}{L_p}, \tag{2.13}$$

where χ_r accounts for radiated energy eliminated from the flame. As the oxygen mass fraction $Y_{O_2,\infty}$ (or the oxygen concentration X_{O_2}) increases, radiation becomes important owing to an increase in soot formation. The total flame heat flux, $\dot{q}''_f = \dot{q}''_{f,cond} + \dot{q}''_{f,rad}$ can be calculated by Eq. (2.12) with an additional increase in B (or T_f) for radiation. For simplicity, it is assumed that B linearly increases with X_{O_2}.

2.2.3 Spread Rate and Flame Width

When the flame passes over the molten polymer, the thickness of the liquid film (on the upper surface of the metal core) starts to decrease due to both pyrolysis by heating and a net drag from the gravity, surface tension, and viscous forces. The latter effect is considered through a descending velocity c_D (mm/s) which increases with decreasing viscous forces. As the oxygen concentration increases, the viscous of the molten layer tends to decrease [12], resulting in a larger c_D. Through a residence time (W_f/V_f), the thickness reduces to zero at the flame tail as

$$\frac{\delta_p}{W_f/V_f} = c_D + \frac{1}{\rho_p L_p}\left[(1-\eta)\dot{q}''_f + h_b\frac{\Delta T_2}{2}\right]. \tag{2.14}$$

This gives an implicit expression for the spread rate as

$$V_f = \frac{W_f}{\rho_p\delta_p L_p}\left[(1-\eta)\dot{q}''_f + h_b\frac{\Delta T_2}{2} + c_D\rho_p L_p\right], \tag{2.15}$$

which increases with the flame width and the heat flux from the flame. Also, the flame width,

$$W_f = \frac{V_f \rho_p \delta_p L_p}{(1-\eta)\dot{q}_f'' + h_b \Delta T_2/2 + c_D \rho_p L_p}, \tag{2.16}$$

increases if the spread rate increases faster than the heat flux from the flame.

In order to solve the spread rate explicitly, Region II ($-W_f < x < 0$) is taken as the control volume, and integrating Eq. (2.4) over it yields

$$A_c \lambda_c \left[\left(\frac{dT}{dx} \right)_0 - \left(\frac{dT}{dx} \right)_{-W_f} \right] - (\rho_c c_c A_c) V_f \Delta T_2 \approx P_c W_f (h_b \frac{\Delta T_2}{2} - \eta \dot{q}_f''). \tag{2.17}$$

If the heat flux from the flame is much larger than the boiling heat transfer in Region II ($\dot{q}_f'' \gg h_b \Delta T$), substituting the flame width from Eq. (2.16) leads to

$$RHS = -\frac{(P_c \rho_p \delta_p L_p) V_f (\eta \dot{q}_f'' - h_b \Delta T_2/2)}{(1-\eta)\dot{q}_f'' + h_b \Delta T_2/2 + c_D \rho_p L_p} \approx -\frac{\eta}{1-\eta} (P_c \rho_p \delta_p L_p) V_f. \tag{2.18}$$

Substituting Eq. (2.7) and Eq. (2.10), a quadratic equation for the spread rate is obtained (shown in the Appendix) as

$$\begin{aligned} &\left[(\rho_c c_c A_o)(T_{ig} - T_a) - \frac{\eta}{1-\eta} (P_c \rho_p \delta_p L_p) + (\rho_c c_c A_c) \Delta T_2 + \frac{P_c l_3^2 \dot{q}_{f,net}''}{2\alpha_c} \right] V_f^2 \\ &- \left(P_c l_3 \dot{q}_{f,net}'' \right) V_f + \frac{(\lambda_c A_c) P_o h_1 (T_{ig} - T_a)}{(\rho_c c_c A_o)} = 0. \end{aligned} \tag{2.19}$$

By neglecting the last small constant term, the spread rate can be solved as

$$V_f \approx \frac{P_c l_3 \dot{q}_{f,net}''}{R + P_c l_3^2 \dot{q}_{f,net}''/2\alpha_c}, \tag{2.20}$$

$$\text{where} \quad R = (\rho_c c_c A_o)(T_{ig} - T_a) - \frac{\eta}{1-\eta} (P_c \rho_p \delta_p L_p) + (\rho_c c_c A_c) \Delta T_2,$$

can be viewed as the resistance to flame spread, which changes slightly with ΔT_2. Note that this approximation solution is derived if the thermal length in the solid phase larger than the length of Region III ($l_3 < \alpha_c / V_f$). The approximate spread-rate for $l_3 > \alpha_c / V_f$ is given in the Appendix. For both cases, the spread rate increases with increasing net heating from Region III, $P_c l_3 \dot{q}_{f,net}''$ given by Eq. (2.9), and the conductivity of the wire core because ΔT_2 is also smaller for a larger conductivity wire.

If the thermal conductivity of the wire core increases, $P_c l_3 \dot{q}''_{f,net}$ becomes larger because the temperature profile in Region III is shallower, leading to both a larger l_3 and a larger $\dot{q}''_{f,net}$, as shown in Eqs. (2.8) and (2.9). Since Eq. (2.14) shows that the residence time (W_f/V_f) is mainly determined by the heat flux from the flame, which is almost a constant under a specific oxygen concentration and only varies slightly with ΔT_2, the flame width increases with increasing spread rate. The increase in the flame width in turn increases l_3 to further increase the spread rate. On the other hand, the conductive heat-loss rate from Region II to I increases with the spread rate, as shown in Eq. (2.7). Eventually, a new thermal balance is reached at a larger flame-spread rate.

As the oxygen concentration increases, the heat flux from the flame increases correspondingly, resulting in a larger spread rate. Moreover, the ignition temperature (T_{ig}) tends to decrease as the oxygen concentration increase, which cause an additional increase in spread rate. If the flame width increases, more radiation reaches Region III and the spread rate increases as well.

2.2.4 Burning Rate and Dripping Conditions

As analyzed above, the molten coating starts to descend by a net drag and pyrolyze due to the heat flux from the flame and high temperature wire core. If the former effect is faster, the liquid polymer may accumulate into a hemi-ellipsoid molten ball in the flame tail, increasing both the contact area with the flame and the burning rate. If the heat flux from the flame is not sufficiently high, the size of the molten ball will further increase to a limit and eventually drop once the gravity exceeds the viscous force and surface tension. Therefore, the burning rate can be expressed as

$$\dot{m} = A_p \rho_p V_f = \frac{\bar{P} W_f}{L_p} \left[(1 + \frac{A_b}{\bar{P} W_f})(1 - \eta)\dot{q}''_f + h_b \frac{\Delta T_2}{2} \right], \tag{2.21}$$

where $\bar{P} \approx (P_o + P_c)/2$ is the average perimeter of the wire, and A_b is the surface area of the molten ball. Comparing with Eq. (2.16) shows

$$A_b = c_D \bar{P} \rho_c L_p \frac{W_f}{(1 - \eta)\dot{q}''_f} \sim \frac{V_f}{(\dot{q}''_f)^2}, \tag{2.22}$$

which increases if the flame width increases faster than the heat flux from the flame. Once A_b exceeds the critical value, the molten ball will drop. The critical size of the molten ball decreases as oxygen concentration increases because of a decrease in viscous forces [12]. Moreover, as the oxygen concentration increases, all c_D, $\dot{q}_f''$, W_f and V_f will increase, so that it is difficult to predict the changes in A_b or dripping frequency.

As the pressure decreases, the heat flux from the flame decreases so that the size of the molten ball is expected to increases and more dripping should occur. Here, a dripping coefficient is introduced in order to consider the dripping effect, $0 < \xi = V_b/A_p l_d \leq 1$ where l_d is the average distance between two drops. A larger ξ means more frequent dripping during spread.

Note that during spread the flame width may oscillate due to the growth and dripping of the molten ball which therefore affects the instantaneous spread rate. If only the average flame width is considered, the dripping frequency is insensitive to the average spread rate, based on the analysis on spread rate in last section.

Chapter 3

Experimental Setup

3.1 Ignition Test

The test platform used in this study is illustrated in Fig. 3.1a and Fig. 3.2 shows the front view of combustion chamber in the ignition experiment. The configuration is similar to previous flame-spread tests [24, 25]. The inner dimensions of the combustion chamber are 365 mm (L) × 260 mm (W) × 180 mm (H). Five types of polyethylene (PE) coated wires and two kinds of core-metal, nickel-chrome (NiCr) and copper (Cu), are adopted in this study as shown in Fig. 3.1b. The dimensions of these sample wires are listed in Table 3.2. The densities and heat capacities of NiCr and Cu are similar, but the ratio of their thermal conductivities is about 1:25 [37], which may play an important role during the ignition and the following flame spread.

A coil heater is used as both a heating source and pilot source, placed in the center of the wire sample to initiate ignition, which heats the wire through both convection (major) and radiation (minor). The diameter of the coil is 5 mm, and it is wrapped around the wire with three different lengths, 12 mm, 20 mm and 30 mm. In order to provide various external heat fluxes, the current imposed in the coil and the heating duration are precisely controlled by a regulated DC power supply (accurate to ±0.01 A) and a digital timer (accurate to ±0.1 s), respectively. When the current is small (<5.5 A) or the environmental pressure is low (< 40 kPa), the temperature of the coil heater is not high enough to cause

Figure 3.1: Photo of test stand (a) test platform, (b) sample wires.

Table 3.1: Configuration of sample wires.

Type[a]	d_c (mm)	δ (mm)	d_o (mm)	A_c (mm^2)	A_p (mm^2)	A_c/A_o
A	0.70	0.15	1.00	0.385	0.401	49%
B	0.50	0.15	0.80	0.196	0.306	39%
C	0.50	0.30	1.10	0.196	0.754	21%
D	0.30	0.20	0.70	0.071	0.314	18%
E	0.30	0.25	0.80	0.071	0.432	14%

[a] Rank of wire conductance: $A > B \approx C > D \approx E$.

ignition before the flammable mixture exceeds the rich limit near the coil heater. In these cases, an additional pilot source is placed above the coil to achieve ignition. The whole ignition process is recorded by a digital video (DV) camcorder (Sony HDR-XR500V, 30 fps) through the side window of the chamber. For all non-spread cases, the mass loss of the wire is measured by an electronic balance (accurate to 0.1 mg).

Near critical conditions, flash or spread may or may not occur under identical heating conditions, because of experimental irreproducibility. Therefore, in order to reduce experimental errors, at least 5 repeated tests are conducted under the same heating condition. The curves for both the flashpoint and the spread point are defined as the 50% chance condition (e.g. 3 times flash/spread and 3

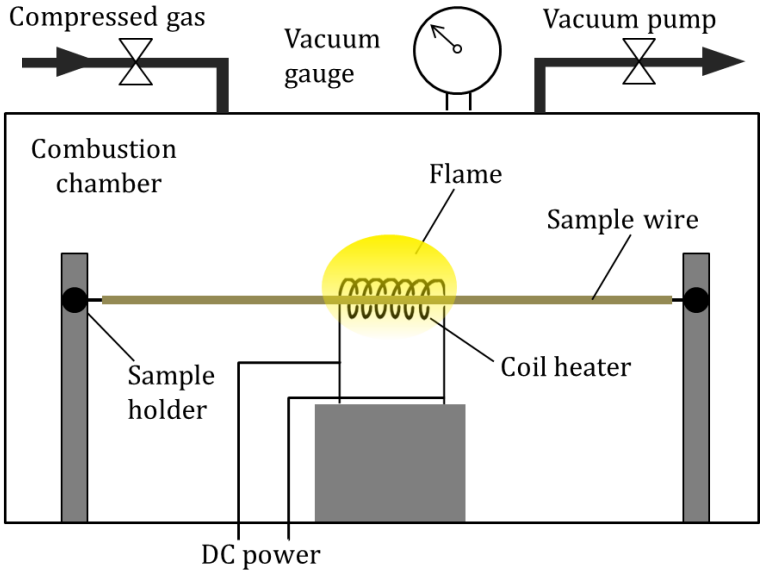

Figure 3.2: Schematic illustration of the combustion chamber in ignition test (front view).

times not flash/spread). In total, over 3000 experiments have been performed in this ignition study.

3.2 Flame-spread Test

The same combustion chamber is adopted in the flame-spread study and Fig. 3.3 shows the front view. The configuration is similar to that described in previous work [24, 25, 38]. The oxygen concentration is varied from 21% (normal atmosphere) to 80% during two sets of tests: (I) constant ambient pressure ($P_a = 1$ atm), and (II) constant oxygen partial pressure (normoxic: $P_{O_2} = 21$ kPa). During the experiment, all gas lines are turned off, without forced flow, and the maximum variation of oxygen concentration, because of oxygen depletion, is estimated to be less than 0.5%.

A coil heater is placed near the end of the wire sample to initiate ignition, resulting in the subsequent flame spread along the wire. The current applied to the heating coil (12 A) and the heating duration (5 sec) are fixed throughout the experiments in order to obtain constant ignition conditions. The entire spread

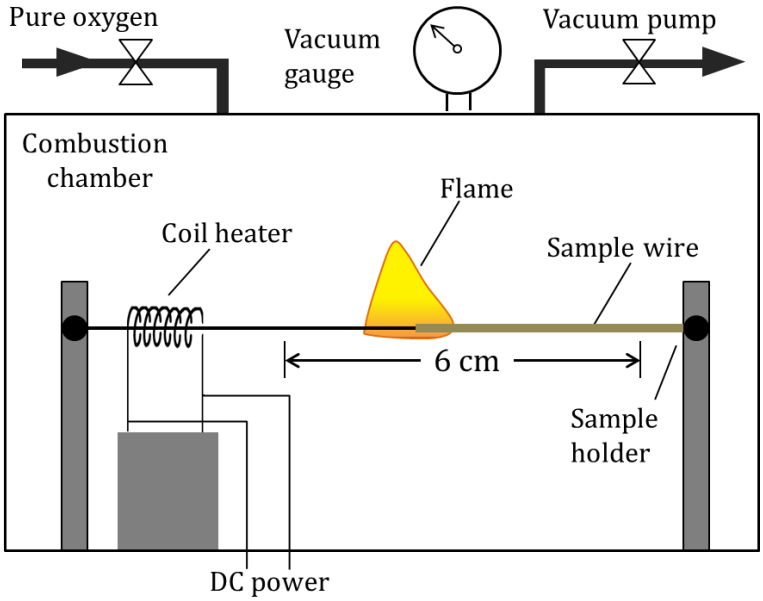

Figure 3.3: Schematic illustration of combustion chamber in flame-spread test (front view).

process is recorded by a digital video (DV) camcorder (Sony HDR-XR500V, 30 fps) through the side window of the chamber. Shooting conditions of the DV camcorder include open-aperture, a shutter speed of 1/500 s, and 3 dB in gain throughout the study. All runs are performed inside a dark room to avoid any possible noise in frames. In oxygen-enrich experiments, the threshold value of the video background is set higher in order to acquire a clearer image of the more-luminous flame. In order to reduce experimental errors, at least 4 tests are repeated under each ambient condition.

Chapter 4

Results and Discussion of Ignition

4.1 Ignition Phenomena

A typical ignition process at normal atmosphere is shown in Fig. 4.1. Once the heater is turned on, the coil soon reaches a high temperature while the sample wire is heated and the PE coating begins to melt and pyrolyze. Then, a blue premixed flame develops, denoted as the flashpoint (Fig. 4.1a), and it grows to a diffusion flame (Fig. 4.1b). Later, the flame separates and begins to propagate in two directions inside the coil heater (Fig. 4.1c). If the imposed heat flux is suddenly reduced (heating power turned off) during this ignition-to-spread transition, the flame may become weaker and extinguish at the end of coil (Fig. 4.1d). Upon continuing to heat the wire after the flash, the weak flame can reach the spread point (Fig. 4.1e). Afterwards, steady-state flame spread can be achieved (Fig. 4.1f). Usually, in experiments a long heating time is required for a high-conductance wire (large thermal conductivity and diameter of wire core), which will be analyzed in the next chapter.

Mass loss measurement shows that for all wires the mass loss right below the spread point is very stable, almost equals to the mass of PE layer inside coil heater. In other words, all fuel in the heating zone is burnt or pyrolyzed before the flame could spread out, which implies an important role of combustion heat from fuel during the ignition-to-spread transition [39]. One the other hand, it is also observed that the mass loss at the flashpoint decreases as the heat flux

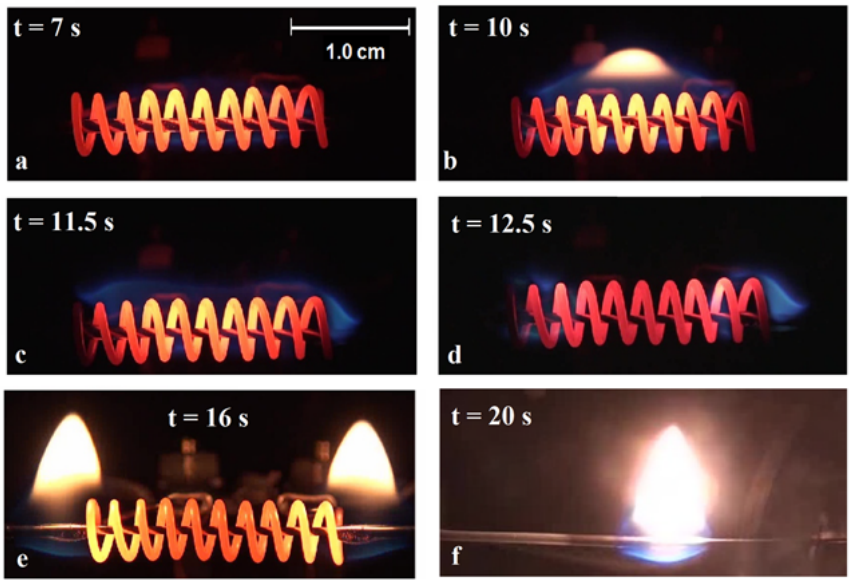

Figure 4.1: The typical ignition process of a NiCr-A wire with $I = 10$ A, a heating time of 6.9 sec and a 2 cm coil heater. (a) flashpoint; (b) fire point; (c) spread inside the heating zone; (d) flame passing through the end of the heating zone; (e) spread point; and (f) steady-state spread.

increases, indicating that the mass loss rate increases with the external heat flux before reaching the critical value for flash [40]. Further reducing the heat flux leads to no flash because the heat flux is too low to achieve the critical mass flux before either all the available fuel is pyrolyzed or a thermal balance for the wire is achieved. Care also needs be taken in the interpretation of the critical mass flux here because the value itself depends on the test configurations [27]. In the current test setup, the distance between the sample wire and the coil heater is small and close to the minimum location of ignition source (comparable to the quenching distance). It is possible that the flammable mixture exceeds the rich-limit before the coil reaches a sufficiently high temperature to ignite the mixture, especially in low pressure cases where the additional mixture by natural convection becomes weak.

4.2 Flashpoint

Fig. 4.2a presents the numerical solutions of Eq. (2.1) with wires of types A-D used in the experiments. A wire core of iron (Fe) was also calculated for type B. The densities and heat capacities of NiCr, Fe, and Cu are similar, but the ratio of their thermal conductivities is about 1:5:25 [37]. The thermal properties of polyethylene were taken from the literature [41]. An ignition temperature of 673 K [28] and a heating length of 20 mm are assumed. Table 4.1 lists the theoretical critical heat flux, $\dot{q}''_{e,crt}$ and the index n, calculated by solving Eq. (2.1) for different values of $\dot{q}''_e$ and fitting the results to Eq. (2.2), for all sample wires.

Comparing three Type-B wires in Fig. 4.2a shows that the critical heat flux and the required heating duration are larger for a wire core with a larger thermal conductivity. For Cu wires, the diameter of the wire core has a strong effect on wire ignition, but the effect is weak for the NiCr or Fe wires as shown in Table 4.1. Comparison between Type B and D wires in Fig. 4.2a indicates that the effect of coating thickness on ignition is small for high heat fluxes, but it increases with decreasing heat flux and affects the critical heat flux by changing the wire cooling condition. Generally, ignition is more difficult to achieve for a higher-conductance wire (higher thermal conductivity, larger diameter, and thinner coating). The index n in Table 4.1 is strongly affected by the thermal conductance, which increases with increasing both conductivity and area-fraction of the wire core, and therefore does not confirm to ideality [28]. Since the diameters of all of the wires are small enough for them to be thermally thin locally, the tendency to approach the ideal thermally-thin limit as the conductance decreases (Table 4.1) can be identified as consequence of the associated reduction in the axial heat loss.

Fig. 4.2b shows the corresponding experimental results with error bars in terms of the heater's current and heating duration. In the experiment, a longer heating duration and a larger minimum heating current are required to achieve flash for a higher-conductance wire, which is the trend predicted by the model in Fig. 6a. Because the actual heat flux reaching the wire is neither a constant nor a linear function of current, further quantitative comparison between experiment and the model is difficult, but comparisons of $\dot{q}''_{e,crt}$ indicates that 6 A and 7 A

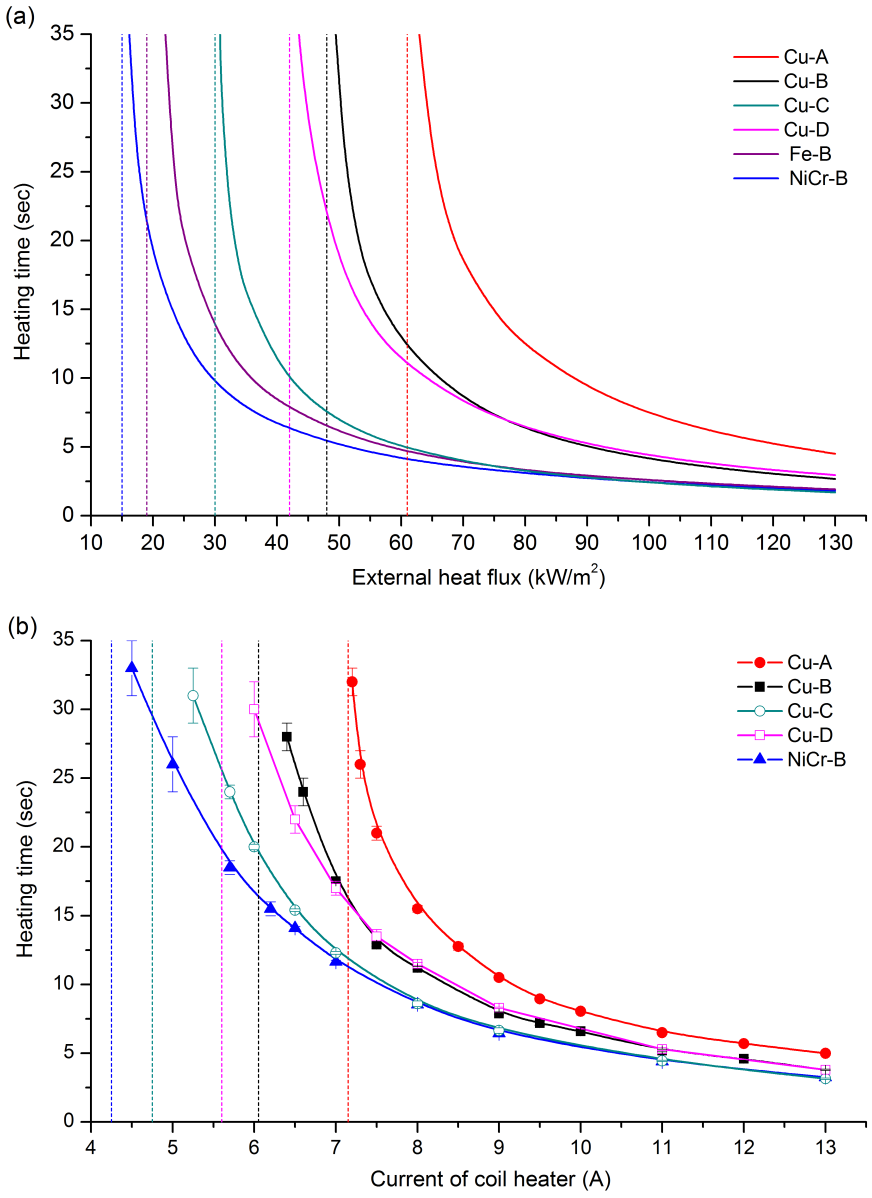

Figure 4.2: Effects of external heat flux on heating time at flashpoint (a)simulation results; (b) experimental results. Dashed lines represent the critical heat flux/ current.

Table 4.1: n and $\dot{q}''_{e,crt}$ (kW/m^2) of sample wires with L =2.0 cm.

Type	Cu		Fe		NiCr	
	n	$\dot{q}''_{e,crt}$	n	$\dot{q}''_{e,crt}$	n	$\dot{q}''_{e,crt}$
A	2.65	61	1.70	23	1.53	17
B	2.95	48	1.79	19	1.57	15
C	2.30	30	1.63	14	1.35	12
D	2.31	40	1.53	17	1.33	14

corresponds roughly to 50 kW/m^2 and 60 kW/m^2 under long-term heating.

4.3 Ignition-to-Spread Transition

According to the analysis in Chapter 2, a large conductive heat loss along the wire core may quench the weak flame during the ignition-to-spread transition, which was observed in experiments (Fig. 4.1d). Measurements showed, as excepted, that when the flame extinguished during the transition phase, the mass loss was nearly a constant and equal to the mass of the PE coating in the heating zone (Δm). To ensure that the weak flame passes through the transition, continuation of wire heating is sometimes required after flash occurs, and the magnitude of the additional heating duration (Δt) is determined by the wire conductance and heating conditions.

From the previously indicated comparisons in Fig. 4.2, we estimate the effective heat flux from a given current through the coil to be $\dot{q}''_e$ from the model for the same ignition time. By integrating Eq. (2.1) and Eq. (2.4), H_{fl} and H_{sp} can be evaluated. Assuming $\eta \approx 5\%$, Δt is then roughly estimated from Eq. (2.6). For a high-conductivity wire, the enthalpy gap ($H_{fl} - H_{sp}$) is expected to be large, requiring a long heating duration to sustain flame spread. As the heat flux decreases, the temperature profile at the flashpoint will broaden, leading to a larger H_{fl}, so that, according to Eq. (2.6), Δt will first increase because of the decrease in $\dot{q}''_e$ and then decrease because of the increase in H_{fl}. Near the critical

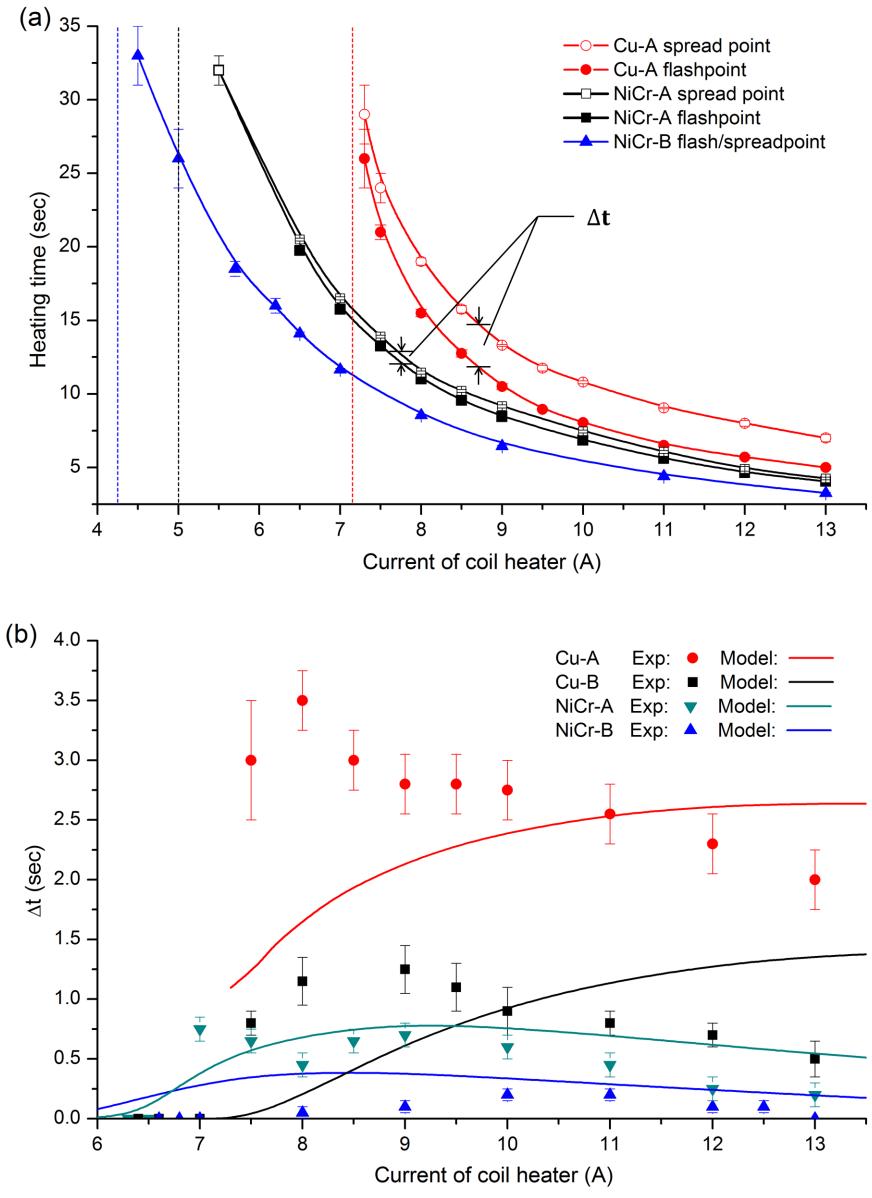

Figure 4.3: (a) flash and spread point in experiment; (b) comparison of Δt between experiment and simulation.

heat flux, the calculated Δt may become negative, meaning that the flashpoint converges to the spread point. Fig. 4.2a shows the experimental spread point of several sample wires, and Fig. 4.2b compares Δt between experiment and model calculation.

Comparison shows that the experimental results generally reflect the model predictions. The average value of Δt increases with wire conductance (Cu-A > Cu-B > NiCr-A > NiCr-B). For the NiCr-B wire, the difference between the flashpoint and spread point is very small (seen in Fig. 4.3b), so only one curve is show in Fig 4.3a. In the experiment, except for the Cu-A wire, under a low current (< 7 A) and a long heating duration (> 20 s), the flame will always spread after the flash, in agreement with the model. In Fig. 4.3b, Δt in high-heat-flux experiments is always lower than the model prediction, probably because after the power is off the hot coil heater continues to heat the wire. On the other hand, in the opposed limit, when the heat flux is low, the wire temperature increases slowly near the ignition temperature, increasing losses so that less of the heat from the coil gets to the wire, and the actual heat flux then decreases, requiring a longer heating time in low-heat-flux experiments than calculated. The dominant effect is that high wire conductance not only makes flash difficult to achieve, but also causes the flame to be more difficult to sustain in the transition phase, which therefore favors greater fire safety from the perspective of ignition.

4.4 Influence Factors on Ignition

4.4.1 Heating Length

The heating length plays an important role in wire ignition. A long heating zone reduces the effect of wire conductance and the value of n, making wires close to being thermally thin. According to Eq. (2.3), with a longer heating length, the critical heat flux is smaller and becomes less dependent on wire conductance. Based on Eq. (2.6), as the heating length increases, H_{fl} and Δm will increase, so ΔQ will also decrease, and finally the spread point will converge to the flashpoint.

Fig. 4.4 compares the ignition curves for Cu-B wire with three different

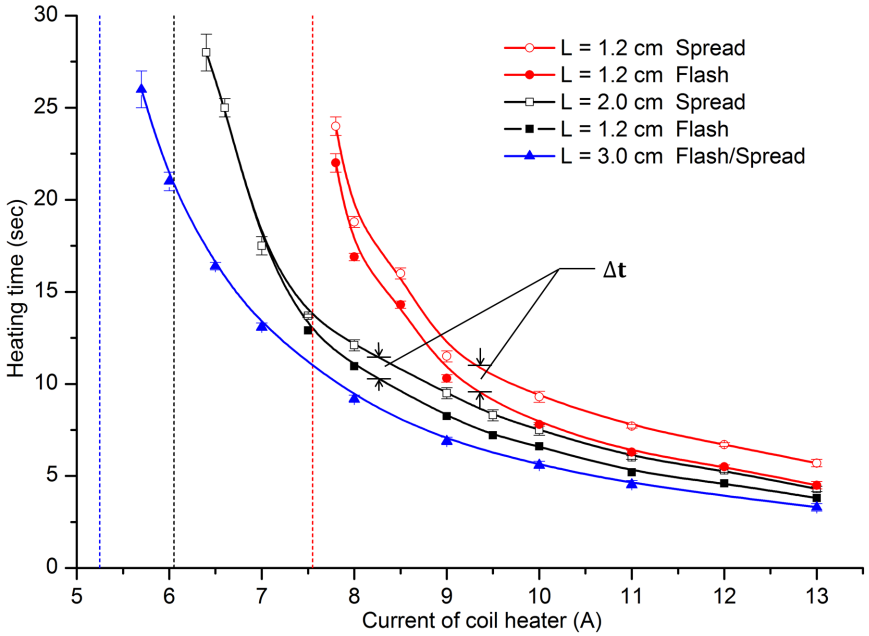

Figure 4.4: Ignition curves for different heating lengths.

lengths of coil heater. Clearly, for a longer heating length the ignition curve is lower, and the minimum heating current is smaller. Also, the additional heating time between flash and spread decreases. With a 3 cm coil heater, as long as flash occurs, the flame will spread. All of these experimental observations are consistent with the model.

4.4.2 Pressure

Fig. 4.5 shows a typical ignition process at reduced-pressure atmospheres. In the low-pressure experiment, the coil heater becomes brighter, but the flash flame becomes less-luminous (blue flame) during ignition (Fig. 4.5a). Once it spreads out, the teardrop-shape flame (Fig. 4.1f) becomes oval or sphere (Fig. 4.5c) [24]. It is also observed that as the heat flux reduces, all fuel in the heating zone can be rapidly pyrolyzed without flash because the fuel-rich mixture is easier to achieve under the lower oxygen partial pressure. This is also supported by the fact that flash occurs in the outer edge of the coil when the molten ball just moves out of the coil [39].

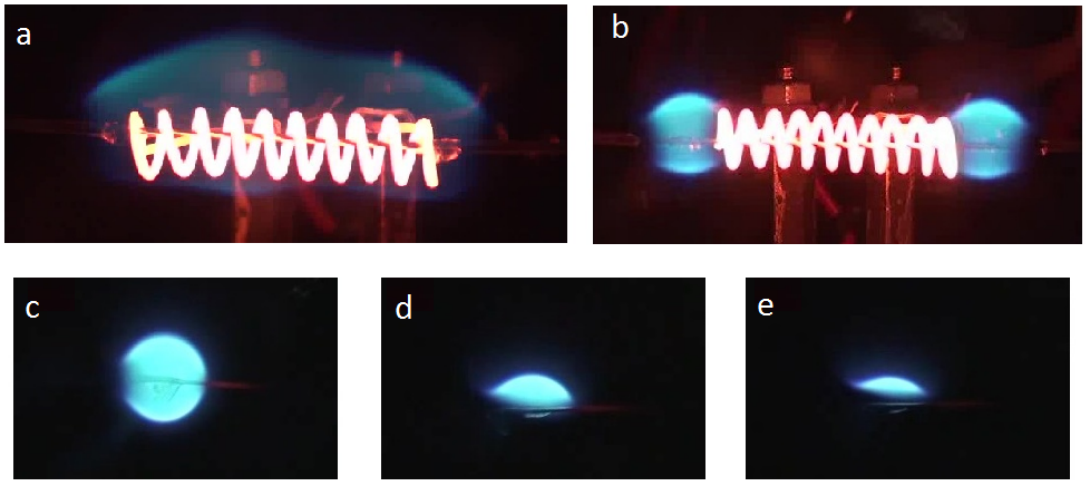

Figure 4.5: The typical ignition process of a NiCr-B wire with a 2 cm coil heater at $P_a = 20$ kPa. (a) flashpoint; (b) flame passing through the end of the heating zone; (c) spread out; and (d)-(e) flame becomes weak, and then, extinguishes.

As the ambient pressure further decreases (< 20 kPa), the natural convection becomes too weak to support the steady flame-spread and the flame extinguishes after spread for a short distance (Fig. 4.5c and d). Nevertheless, no a minimum/critical flash pressure is found in experiment. Considering the definition of the flashpoint, the flash will occur as long as heat flux is high enough and the gas mixture is within the flammability limit. Although the fuel may be too rich to exceed the fuel-rich limit, a long-time mixture in the chamber will guarantee the occurrence of a strong flash or an strong explosion. In experiment, when the pressure is lower than 10 kPa, a strong flash is observed under a large heat flux, which has a long flame length, even reaching the top of the chamber.

As the environmental pressure decreases, natural convection becomes weaker, resulting in a smaller heat loss from the wire. According to the model for the flashpoint, the ignition time at a given heat flux will decrease with decreasing pressure, implying a higher risk of fire. Similarly, an easier ignition is expected in microgravity environments, agreeing with the results of ignition by short-term excess electric current in Fujita et al. [15]. Fig. 4.6a. compares the solutions of Eq. (2.1) under normal and reduced-pressure atmospheres, and the dashed line represents the limiting case in microgravity where no natural convection exists, agreeing with

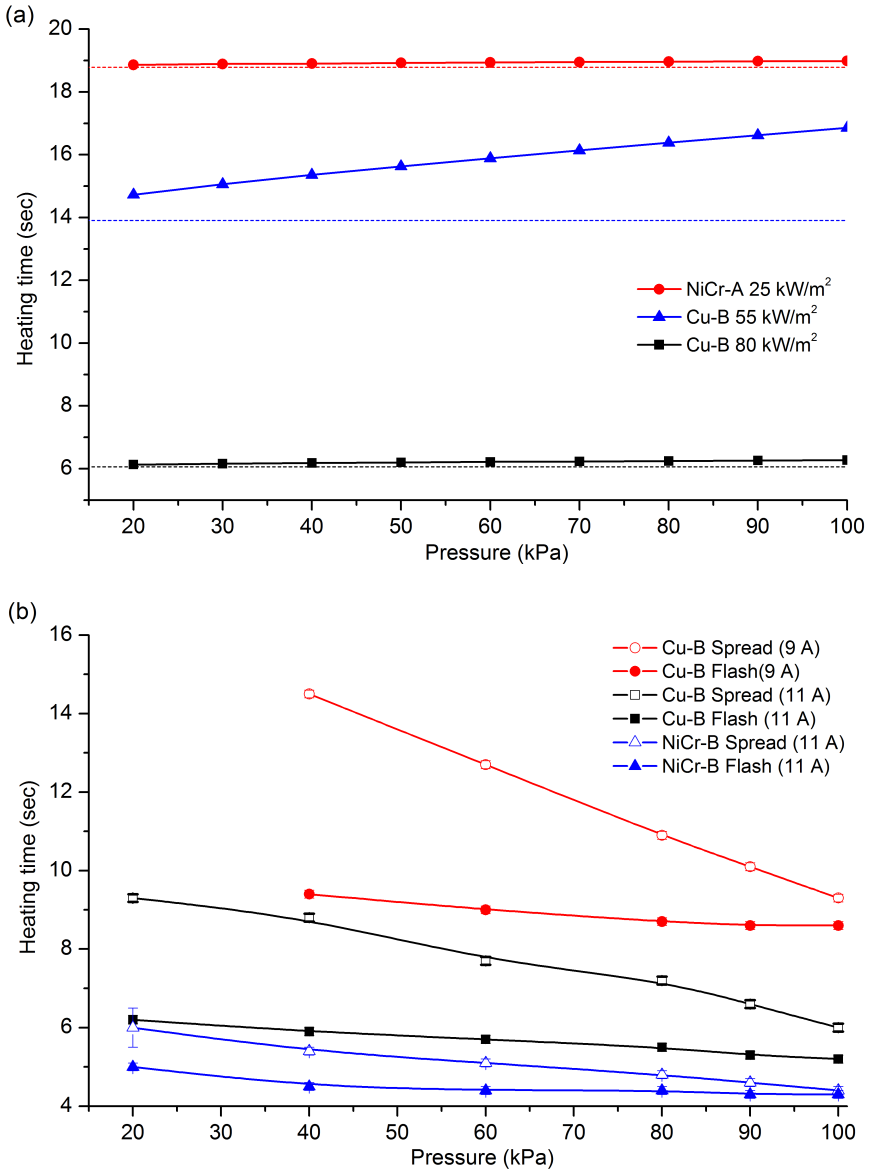

Figure 4.6: Ignition time at reduced pressures with a 2 cm coil heater: (a) numerical results of flashpoint; (b) experimental results of flashpoint and spread point.

above analysis. The change of heating time under different pressures increases with increase of wire conductance and decrease of external heat flux. But in general, the effect of pressure or gravity on the flashpoint is estimated to be small compared with the influence of wire conductance or heating length. However, according to Eq. (2.6), Δt in the ignition-to-spread transition is expected to increase with decreasing pressure for two reasons: (1) both the flame spread rate and flame width increase slightly as pressure decreases [25], resulting in a larger enthalpy in spread (H_{sp}); (2) the flame becomes weaker at reduced pressures, leading to a lower heating efficiency (η).

Fig. 4.6b shows the experimental results at reduced pressures, demonstrating that the heating duration for the flashpoint actually increases slightly as pressure decreases, contrary to the preceding prediction. This occurs because, as the pressure decreases, the convective heat transfer between the coil and wire decreases, resulting in a smaller effective heat flux. It also explains the coil in low-pressure experiment becomes much brighter under the same heating duration (Fig. 4.5a). On the other hand, the gap of heating time between the flashpoint and spread point significantly increases, as predicted. Considering that H_{sp} at reduced pressures only increases slightly with spread rate and flame width, a large drop in heating efficiency from the weaker flame is likely to be the major reason for such a large increase in Δt as pressure decreases. This experiment strongly suggests that in practice when studying the difficulty of ignition, changes in ignition and heating sources with experimental conditions cannot be neglected.

4.4.3 Oxygen Concentration

As the oxygen concentration (X_{O_2}) increases, ignition may become easier, possibly aided by oxidative pyrolysis [12]. The flame also becomes stronger and increases η, decreasing the additional heating duration between the flashpoint and spread point. Fig. 4.8 shows how the heating time changes with oxygen concentration at both normal atmospheric pressure and reduced pressures. Both the heating time at flashpoint and the additional heating time to spread point decrease with increasing oxygen concentration, as predicted. At reduced pressure, the heating

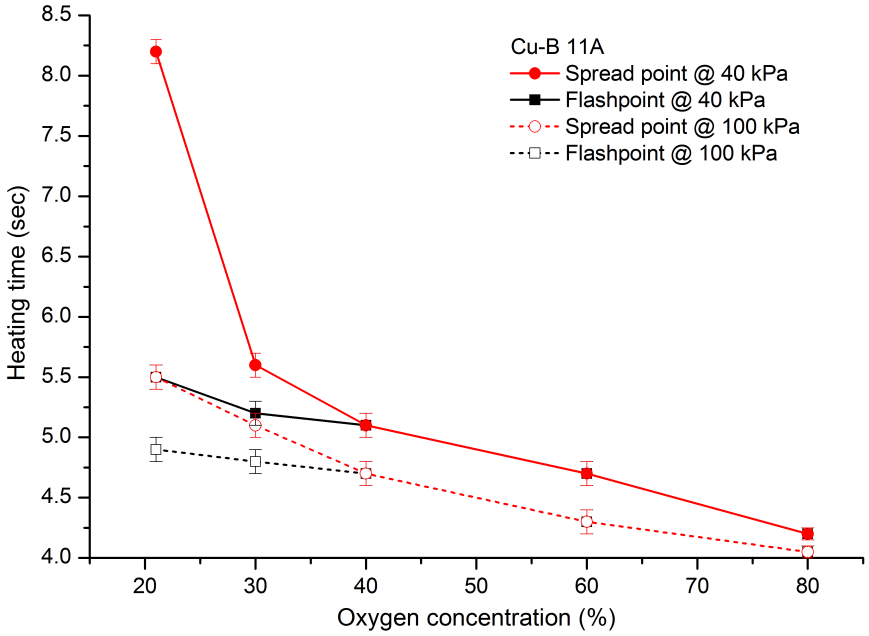

Figure 4.7: Experimental results at oxygen-enriched atmosphere with a 2 cm coil heater.

duration is relatively longer because the heating efficiency of the coil decreases as discussed above. Once $X_{O_2} > 40\%$, spread occurs as soon as the flashpoint is reached for all sample wires.

During experiment, the ignition delay ($t_{ig} > t_h$)) is also observed when $X_{O_2} > 50\%$. Fig. 4.8 shows a typical ignition delay at $X_{O_2} = 80\%$ when the heating time is near the flashpoint. It is observed that 5 sec after the end of the heating (Fig. 4.8a), the coil is cooling down (Fig. 4.8b). Afterward, continuous strong flashes occur (Fig. 4.8c-d), leading to flame spread (Fig. 4.8e-f). Upon increasing the heating time, the flash will occurs right after. The ignition delay was also observed in ignition experiment by short-term excess electrical current in drop town experiment [15]. In that case, ignition occurs after the end of applied current due to a longer mixing time in microgravity environment, and the delay time increases as the current decreases. All of these indicate that the heat-transfer-based ignition model is no longer appropriate in excessive oxygen-enriched atmosphere, and both mixing and chemical kinetics in the gas phase may become important in controlling the ignition and spread of fires.

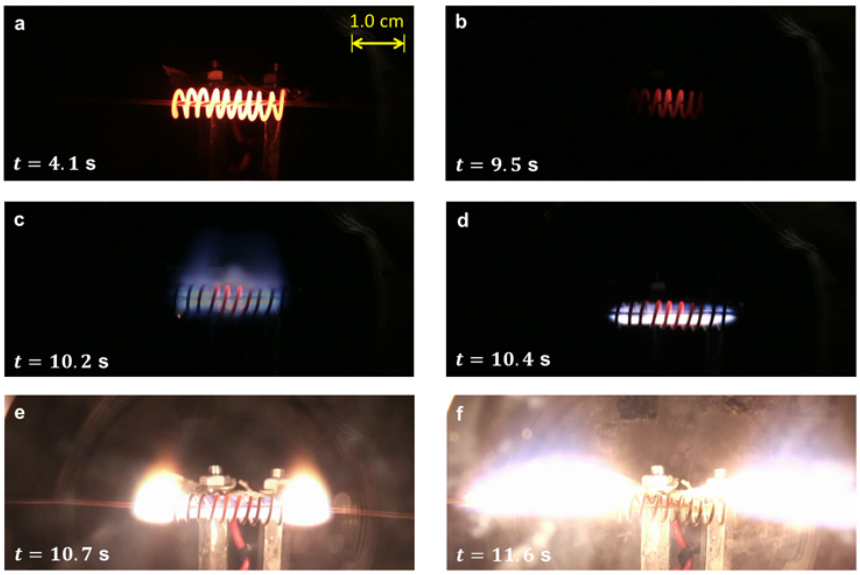

Figure 4.8: The ignition delay process of a Cu-B wire $I = 11$ A, a heating time of 4.1 sec and a 2 cm coil heater at $P_a = 1$ atm, $X_{O_2} = 80\%$ (ignition delay). (a) hot coil at the end of heating time; (b) coil cools down after heating; (c) first flash; (d) second flash; (e) spread point; (f) strong flame.

Chapter 5

Results and Discussion of Flame Spread

5.1 Flame-Spread Phenomena

5.1.1 Flame Shape

Fig. 5.1 shows the detailed flame structures and burning conditions for Cu-C and NiCr-C wires at ambient atmospheric conditions. In general, the flame (yellow) width for the Cu wire is longer than that for the NiCr wire. For Cu wires, the lengths of both the blue flame downstream and the molten polymer region upstream are comparable to the width of the yellow flame and are much longer than those for NiCr wires. Tiny bubbles are generated on the surface of the wire core within the flame zone, and a drastic bubbling process occurs inside the molten ball for both wires. It is also observed that the flame at the leading edge, tail and that below the wire are always non-luminous (blue flames) because buoyancy stretches the flow field upward, suppressing soot formation below [25].

Figs. 5.2 and 5.3 show typical instantaneous flames (located about 4 cm away from the coil heater), under different oxygen concentrations (21% - 80%) and pressures (Set I: $P_a = 1$ atm and Set II: $P_{O_2} = 21$ kPa), spreading over Type B and D sample wires, respectively. The flame becomes much brighter in oxygen-enriched atmospheres, even under reduced pressures (normoxic). In order to record a clear

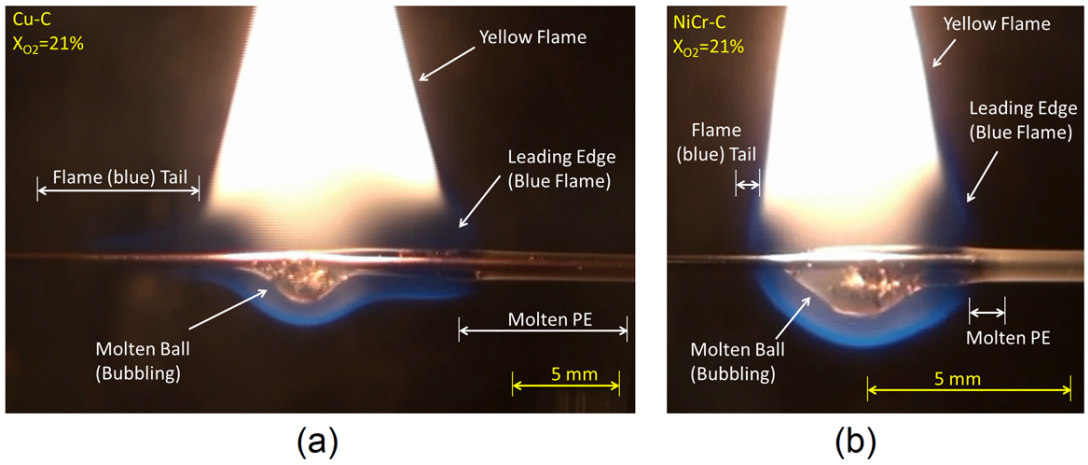

Figure 5.1: Flame structure at normal atmosphere (P_a = 1 atm, X_{O_2} = 21%): (a) Cu-C wire; (b) NiCr-C wire.

flame image, the background filter has to be set higher while it becomes difficult to observe the blue flame in either the flame tip or the tail.

As the oxygen concentration increases, the flame height may first increase, and then decreases at the normal atmospheric pressure (1 atm) while it continues to decrease at the reduced-pressure atmosphere. Under the same oxygen concentration, the flame height at the reduced-pressure atmosphere is less than the corresponding value at 1 atm, which is expected due to the reduced natural convection. In addition, at the reduced-pressure atmosphere, the flame width for the Cu wires is smaller than that at 1 atm, but for the NiCr wires, the flame width tends to be longer. The glowing (red-colored) bare wire behind the visible flame tail is observed for NiCr wires, and it becomes pronounced as the oxygen concentration increases. This domonstrates that the peak temperature in the wire core is not inside the flame (Region II), but at a distance away from the flame tail (Region III) by achieving a thermal balance between the flame radiation and the surface reradiation as well as the natural convective cooling, which also implies the importance of the radiation from the flame. No glowing point is observed in those high-conductance Cu wire, possibly due to a shallow temperature profile, discussed in Section 2.2.1.

At high oxygen concentrations (X_{O_2} = 80%, P_{O_2} = 21 kPa and P_a = 26.3

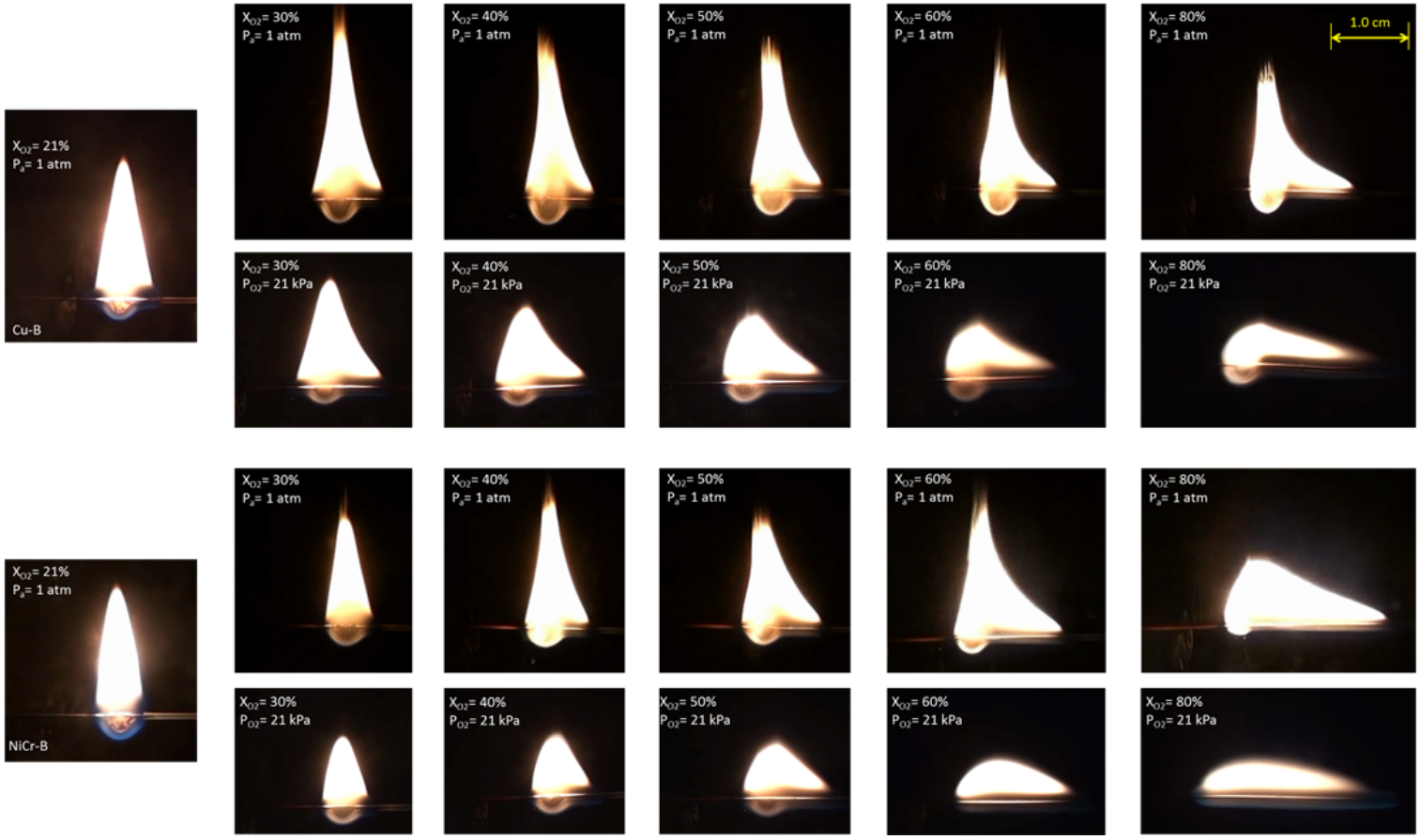

Figure 5.2: Instantaneous flame shapes during spread over Cu-B wires (upper) and NiCr-B wires (lower) at different oxygen concentrations (Set I: $P_a = 1$ atm and Set II: $P_{O_2} = 21$ kPa).

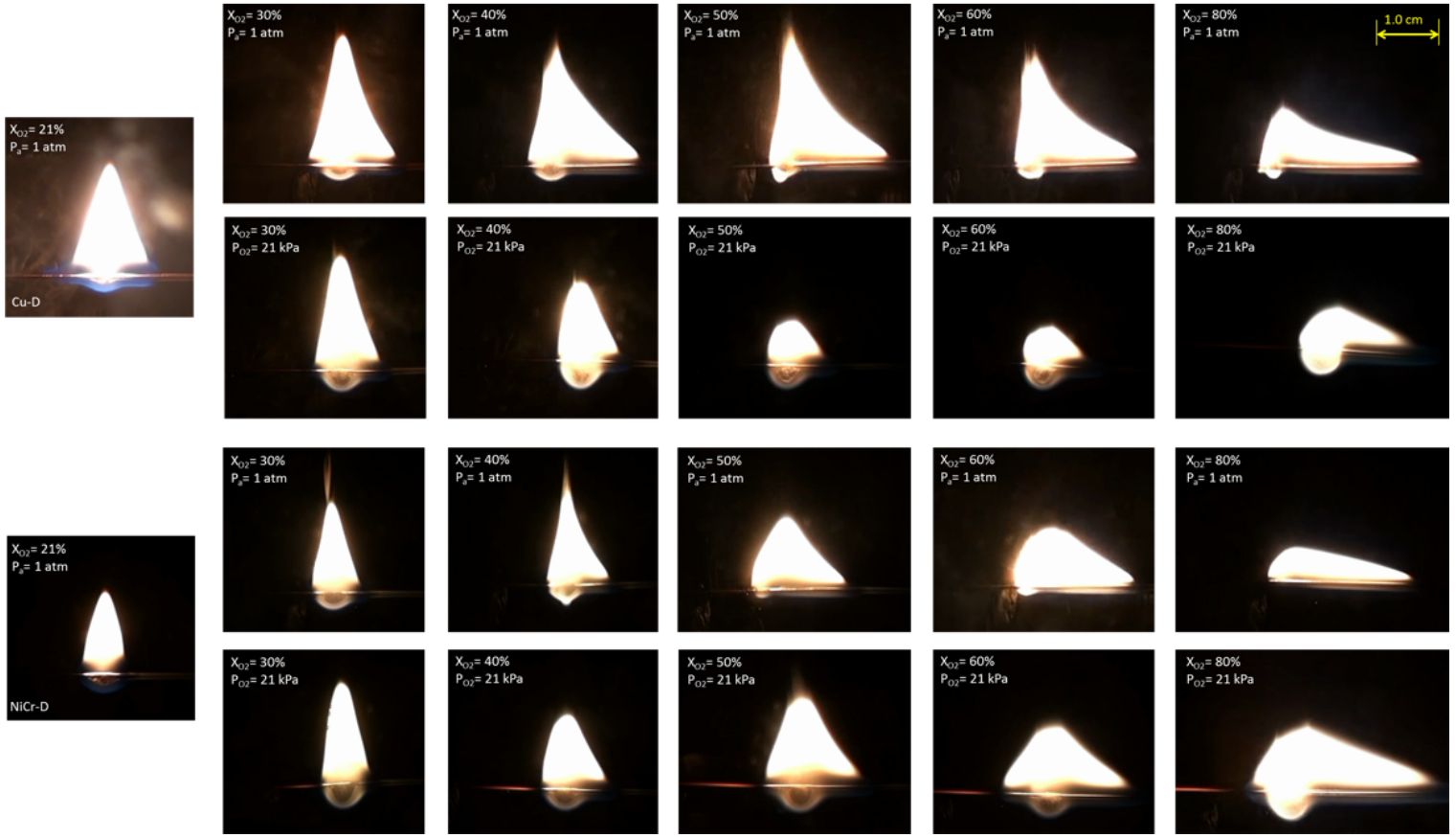

Figure 5.3: Instantaneous flame shapes during spread over Cu-D wires (upper) and NiCr-D wires (lower) at different oxygen concentrations (Set I: $P_a = 1$ atm and Set II: $P_{O_2} = 21$ kPa).

Table 5.1: The experimental and normalized (with respect to the A-Type wire) spread rates with the corresponding ratios for $1/d_o$ and A_c under normal atmospheric conditions ($X_{O_2} = 21\%$, $P_a = 1$ atm).

Type	V_f (mm/s)		W_f (mm)		$\overline{V_f} = V_f/V_{f,A}$		Normalized ratio	
	NiCr	Cu	NiCr	Cu	NiCr	Cu	$\overline{d_o^{-1}}$	$\overline{A_c}$
A	1.62	2.88	5.54	11.94	1.00	1.00	1.00	1.00
B	2.36	3.44	5.50	9.62	1.46	1.19	1.25	0.51
C	1.68	2.13	6.72	11.37	1.04	0.74	0.91	0.51
D	3.03	3.69	5.92	7.68	1.87	1.28	1.43	0.18
E	–	3.16	–	9.00	–	1.09	1.25	0.18

kPa), all of the Cu-E wires and about half of the Cu-D wires broke during flame spread, but rare of them broke up under $X_{O_2} = 80\%$ and $P_a = 1$ atm. On the other hand, a few NiCr-D wires broke at $X_{O_2} = 80\%$ and $P_a = 1$ atm, but rare of them broke at $X_{O_2} = 80\%$ and $P_{O_2} = 21$ kPa. As the ambient oxygen concentration increases, the flame radiation increases and consequently the maximum temperature of the wire core (T_{max}) increases. In addition, as the ambient pressure decreases, the convective heating from the flame becomes relatively weaker, but the convective cooling in Region III also decreases. For Cu wires, the reduced convective cooling is dominant and causes T_{max} to reach the molting temperature of copper ($\sim$ 1385 K [37]), breaking the wire. Fewer NiCr wires broke at reduced pressures because it has a higher melting temperature ($\sim$ 1700 K [37]), and few fuels are left and continues to burn in Region III at $X_{O_2} = 80\%$ and $P_a = 1$ atm (not at $X_{O_2} = 80\%$ and $P_{O_2} = 21$ kPa), rising the core temperature and breaking the wires.

5.1.2 Measurements of Spread Rate and Flame Width

The flame-spread rate is calculated by tracking the time-history of the flame-tip position during the 6 cm semi-steady spread region. Typical time-

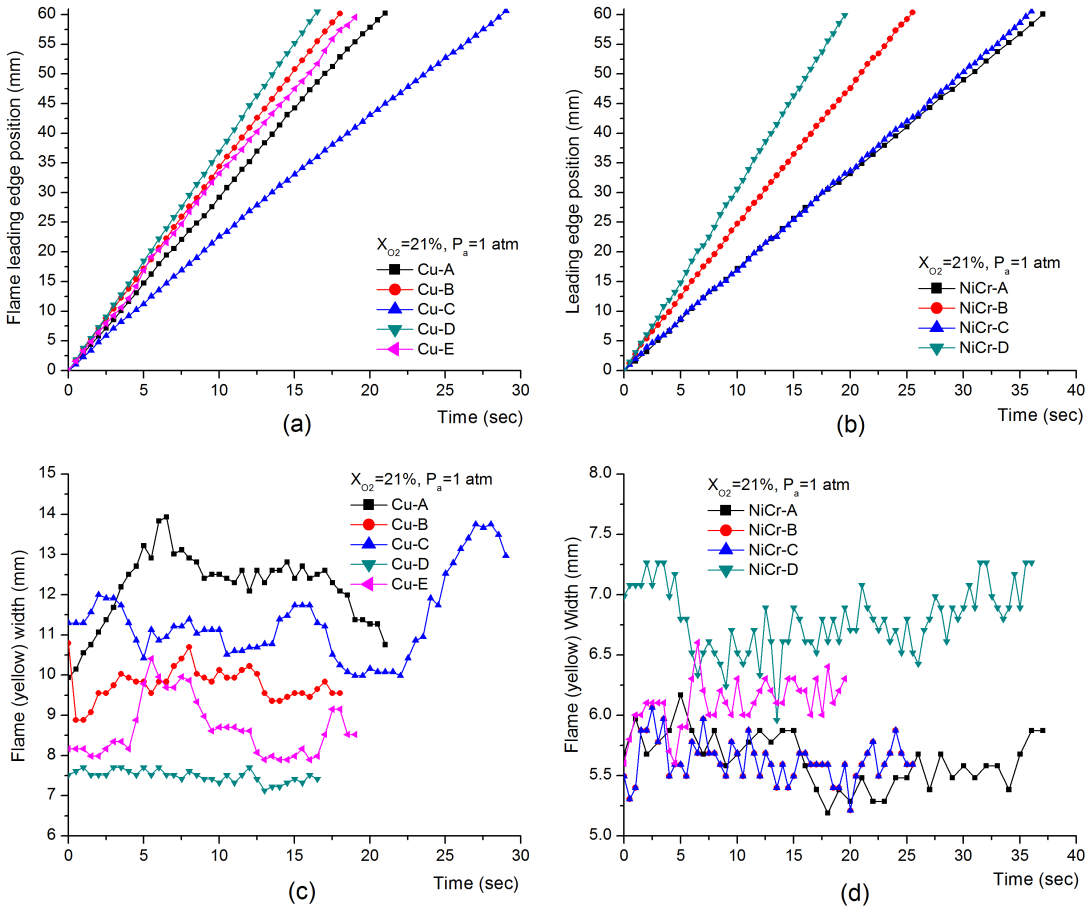

Figure 5.4: At normal atmospheric conditions ($P_a = 1$ atm, $X_{O_2} = 21\%$), the time-history of flame leading edge position, (a) Cu wires and (b) NiCr wires, and the flame (yellow) width, (c) Cu wires and (d) NiCr wires, during the spread event.

histories of flame-tip position and flame (yellow) width at ambient atmospheric conditions for all sample wires are plotted in Fig. 5.4 and at oxygen-enriched atmospheres for Type B wires in Fig. 5.5. It is observed that the flame width oscillates during the initial growth phase after ignition as well as the growth and the motion of the molten ball, so only the average value is considered. On the contrary, the spread rate varies little during the spread process in all cases and can be recognized as an eigenvalue of the system. In other words, the spread rate is relatively insensitive to changes in the flame width and dripping conditions during spread. In addition, both the flame-spread rate and the flame width increase with increasing oxygen concentration.

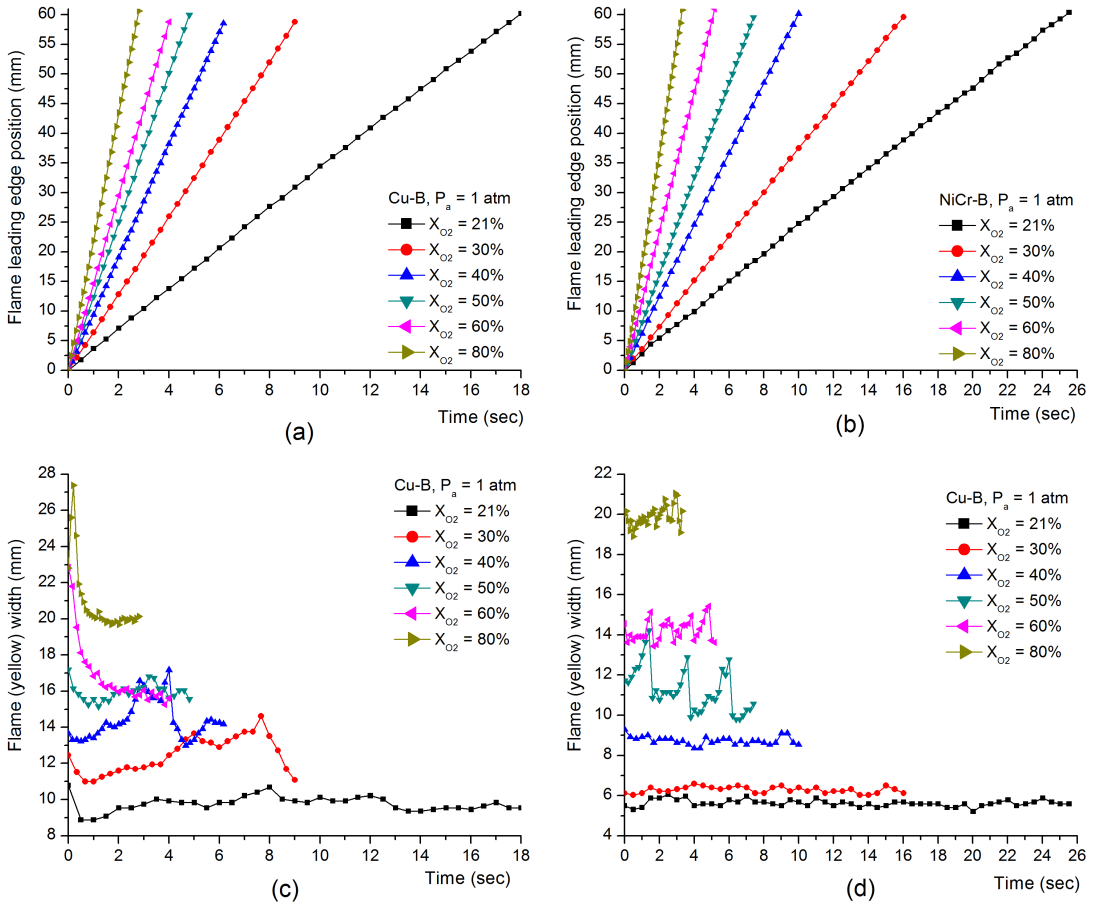

Figure 5.5: In an oxygen-enriched atmosphere ($P_a = 1$ atm), the time-history of flame leading edge position: (a) Cu-B wires and (b) NiCr-B wires, and flame (yellow) width, (c) Cu-B wires and (d) NiCr-B wires, during the spread event.

According to the recorded time-history of the flame-tip position, the average spread rate of four repeated tests under normal atmospheric conditions ($X_{O_2} = 21\%$, $P_a = 1$ atm) are listed in Table 5.1. Also listed are the average flame width, the ratio of the spread rate to that of experiment type A, and the corresponding ratios for $1/d_o$ and A_c. The uncertainties are less than ± 0.1 mm/s for these measured spread rates and less than ± 0.3 mm for flame widths.

Figs. 5.6 and 5.7 compare the flame-spread rate and the flame width between NiCr and Cu wires in oxygen-enriched environments under both test Set I ($P_a = 1$ atm, soild line) and II ($P_{O_2} = 21$ kPa, dash line) conditions, which will be discussed in the following section.

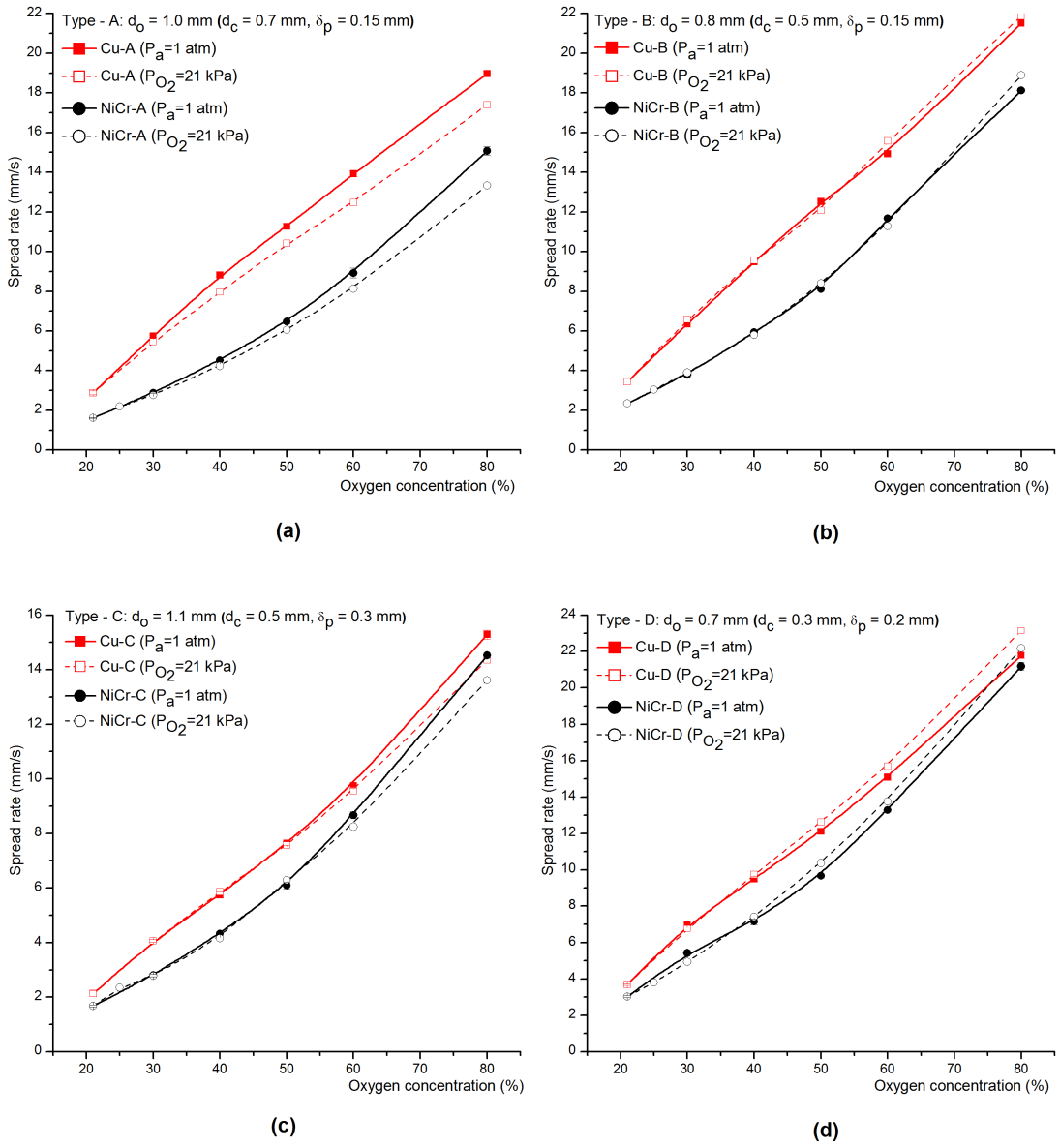

Figure 5.6: Flame-spread rates at various oxygen concentration in test Set I (P_a = 1 atm, solid line) and II (P_{O_2} = 21 kPa, dash line): (a) A-Type wire, (b) B-Type wire, (c) C-Type wire, and (d) D-Type wire.

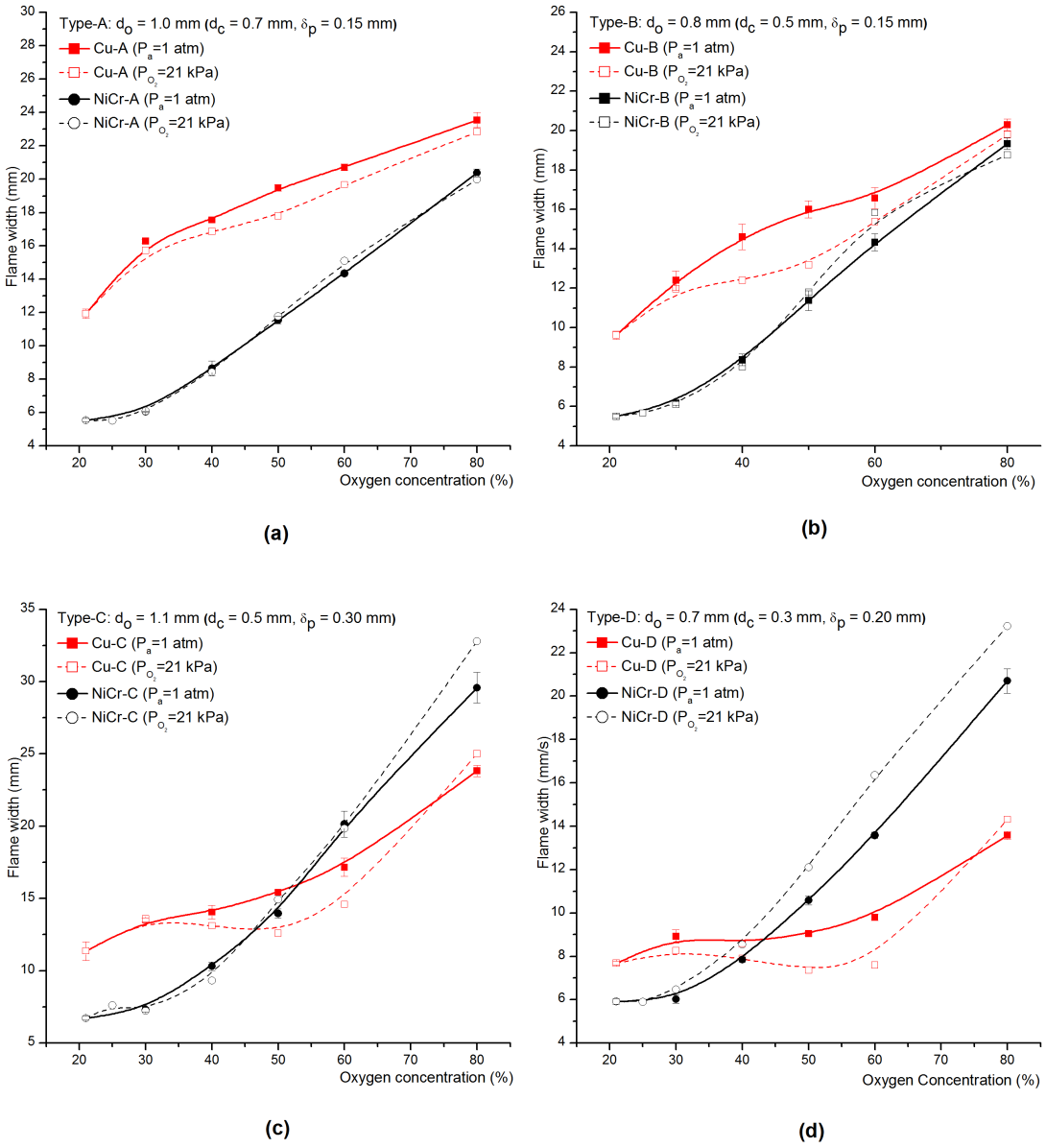

Figure 5.7: Flame widths at various oxygen concentration in test Set I ($P_a = 1$ atm, solid line) and II ($P_{O_2} = 21$ kPa, dash line): (a) A-Type wire, (b) B-Type wire, (c) C-Type wire, and (d) D-Type wire.

5.2 Discussions

5.2.1 Conductivity Effect

According to Table 5.1, at normal atmospheric conditions both the spread rate and the flame width for each Cu wire are larger than those for NiCr wire of the same type, and the differences varies with wire dimensions. Based on the spread model in Section 2.2, the flame-spread rate is predicted by

$$V_f \approx \frac{P_c l_3 \dot{q}''_{f,net}}{R + P_c l_3^2 \dot{q}''_{f,net}/2\alpha_c}, \tag{2.20}$$

$$\text{where} \quad R = (\rho_c c_c A_o)(T_{ig} - T_a) - \frac{\eta}{1-\eta}(P_c \rho_p \delta_p L_p) + (\rho_c c_c A_c)\Delta T_2,$$

so that the spread rate increases with increasing conductivity. Comparison shows that the thermal conductivity of the wire core can affect the spread rate on the same order as the dimension of the wire, and has a large effect on the flame width.

As the oxygen concentration increases, the flame heat flux as well as $l_3 \dot{q}''_{f,net}$ increases, resulting in a larger spread rate for all tested wires (Fig. 5.6). Also, the flame width increases with oxygen concentration, and comparisons show that the flame width for NiCr wire increases faster than that for Cu wire. For NiCr-C and NiCr-D wire, the flame width eventually exceeds those for Cu wires, which may relate to the dripping conditions, to be discussed in Section 5.2.4. Also note that the spread-rate difference between Cu and NiCr wires first increases, and then slightly decreases for all cases. As the flame heat flux first increases, $P_c l_3^2 \dot{q}''_{f,net}/2\alpha_c$ in the dominator of Eq. (2.20) also increases to enlarge the spread-rate difference between the two wires. Further increase in the oxygen concentration will increase the flame width as well as l_3 for NiCr wires (Fig. 5.7), which tends to compensate the conductivity effect, reducing the spread-rate difference.

In order to better compare the differences in spread rate, Fig. 5.8 shows the spread-rate ratio of Cu wires to NiCr wires under various oxygen concentrations. As the oxygen concentration increases, the ratio first increases, and then decreases, which peaks around $X_{O_2} = 30 \sim 40\%$ for all tested wires. Note that this oxygen-concentration range is usually adopted in space applications, making

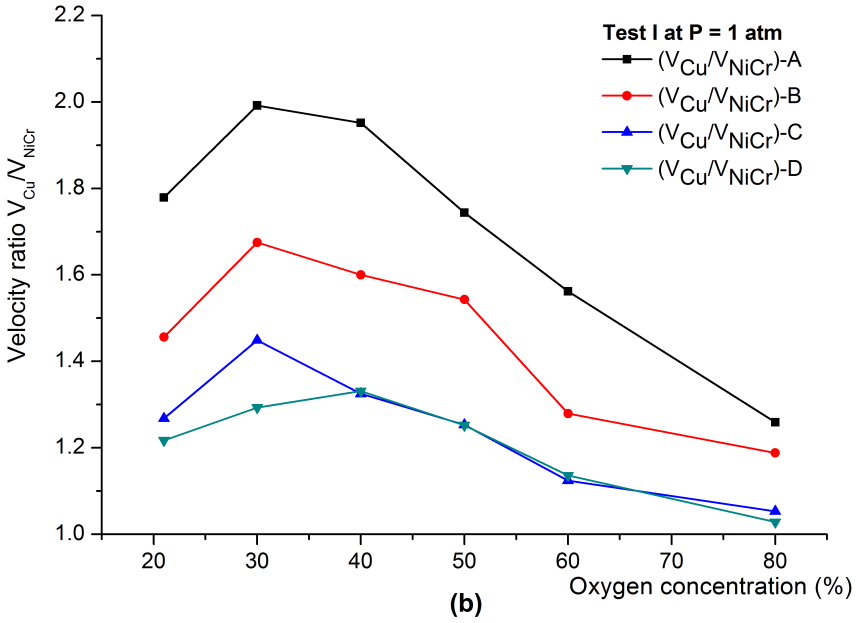

Figure 5.8: The spread-rate ratio of Cu wires to NiCr wires under various oxygen concentrations.

the high-conductivity wire relatively more fire hazardous than at the normal oxygen concentration. Further increasing the oxygen concentration, the conductivity effect becomes small, and the increase in flame heat flux dominates the spread rate.

5.2.2 Wire-Dimension Effect

Under normal atmospheric conditions, the ranks of the spread rate for both NiCr and Cu wires almost follows with the rank of the reciprocal of outer diameter (d_o^{-1}), as shown in Table 5.1. According to an alternate expression for the spread rate,

$$V_f = \frac{W_f}{\rho_p \delta_p L_p}\left[(1-\eta)\dot{q}_f'' + h_b \frac{\Delta T_2}{2} + c_D \rho_p L_p\right], \tag{2.15}$$

the spread rate increases with $\dot{q}_f''$ which decreases with increasing wire outer diameter, $\dot{q}_{f,cond}'' \sim d_o^{-(\mu+1)}$ with $0 < \mu < 1$, as discussed in Section 2.2.2. This generally agrees with the experimental data for low-conductivity NiCr wires, except for the spread rate of NiCr-C which is underestimated because it has a larger flame width

than other NiCr wires. For the Cu wires, the normalized (with respect to Cu-A) spread rate is less than the corresponding d_o^{-1} possibly because the spread rate for Cu-A wire is increased more by its larger conductance.

In order to better describe the influence of the wire dimension, Fig. 5.9 and 5.10 show the experimental as well as the normalized spread rates for NiCr and Cu wires under oxygen-enriched atmospheres (Set I test: $P_a = 1$ atm). Fig. 5.11 compares the flame widths for different wires at both the normal atmospheric and normoxic pressures. The flame width for NiCr-A/B/D wires are almost the same at different oxygen concentrations under both the normal atmospheric or normoxic pressures, which change little if $X_{O_2} < 30\%$, and then monotonically increases once $X_{O_2} > 30\%$. The Flame width for the NiCr-C wire is larger because of a longer residence time for a thicker coating. The flame-spread rate for each wire clearly increases faster than the linear increase in the oxygen concentration because both the flame heat flux and the flame width increase. For the low conductivity NiCr wires, the wire dimension continues to control the spread rate in oxygen-enriched atmospheres so that the rank of the spread rate ($D > B > A > C$) is consistent with the rank of d_o^{-1}, as shown in Fig. 5.9b.

For high-conductivity Cu wires, the flame widths for Cu-A and Cu-B wires increases monotonically with increasing X_{O_2}. On the other hand, the flame widths of Cu-C/D/E wires change only slightly at $X_{O_2} < 60\%$, and then monotonically increase once $X_{O_2} > 60\%$, which may relate to the frequent dripping observed in experiments. Comparing this to NiCr wires, the increase in the flame width for Cu wires is much slower. The spread rates for Cu wires almost increase linearly with oxygen concentration, which is slower than that for NiCr wires, possibly because of a slower increase in the flame width. As the oxygen concentration increases up to 60%, the rank of the spread rate changes to $D \approx B > A > E > C$ from $D > B > E > A > C$ under normal atmospheric conditions, no longer exactly following d_o^{-1}. The spread rates for Cu-D and Cu-E wires increases slower because of the slow increase in the flame width.

Comparing Cu-B to Cu-C wires, their conductance are similar (same core diameter), flame spreads faster over Cu-B because d_o^{-1} is small. Also, comparing

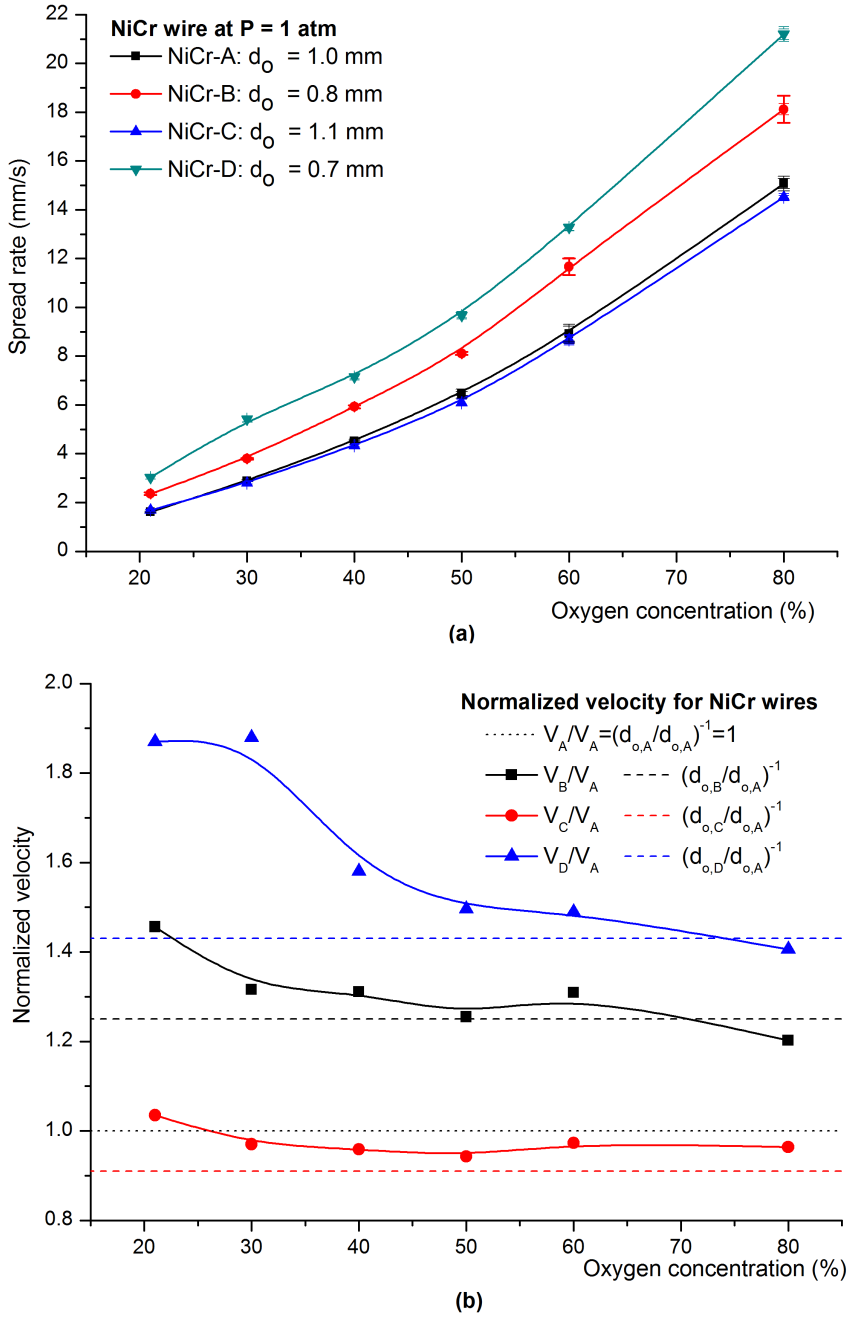

Figure 5.9: (a) Rates of flame spread over NiCr wires for different oxygen concentrations ($P_a = 1$ atm); (b) normalized spread rate with respect to NiCr-A wire.

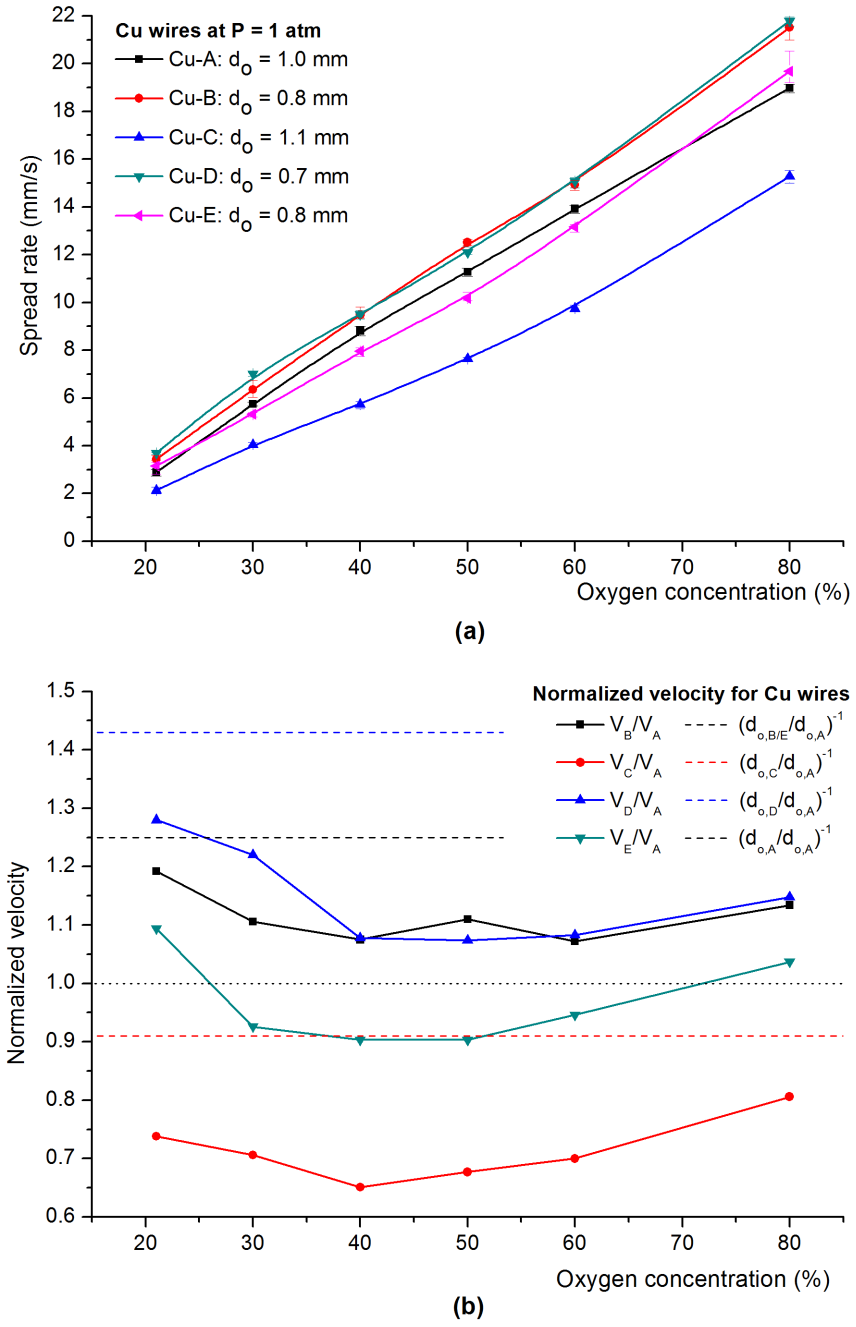

Figure 5.10: (a) Rates of flame spread over Cu wires for different oxygen concentrations ($P_a = 1$ atm); (b) normalized spread rate with respect to Cu-A wire.

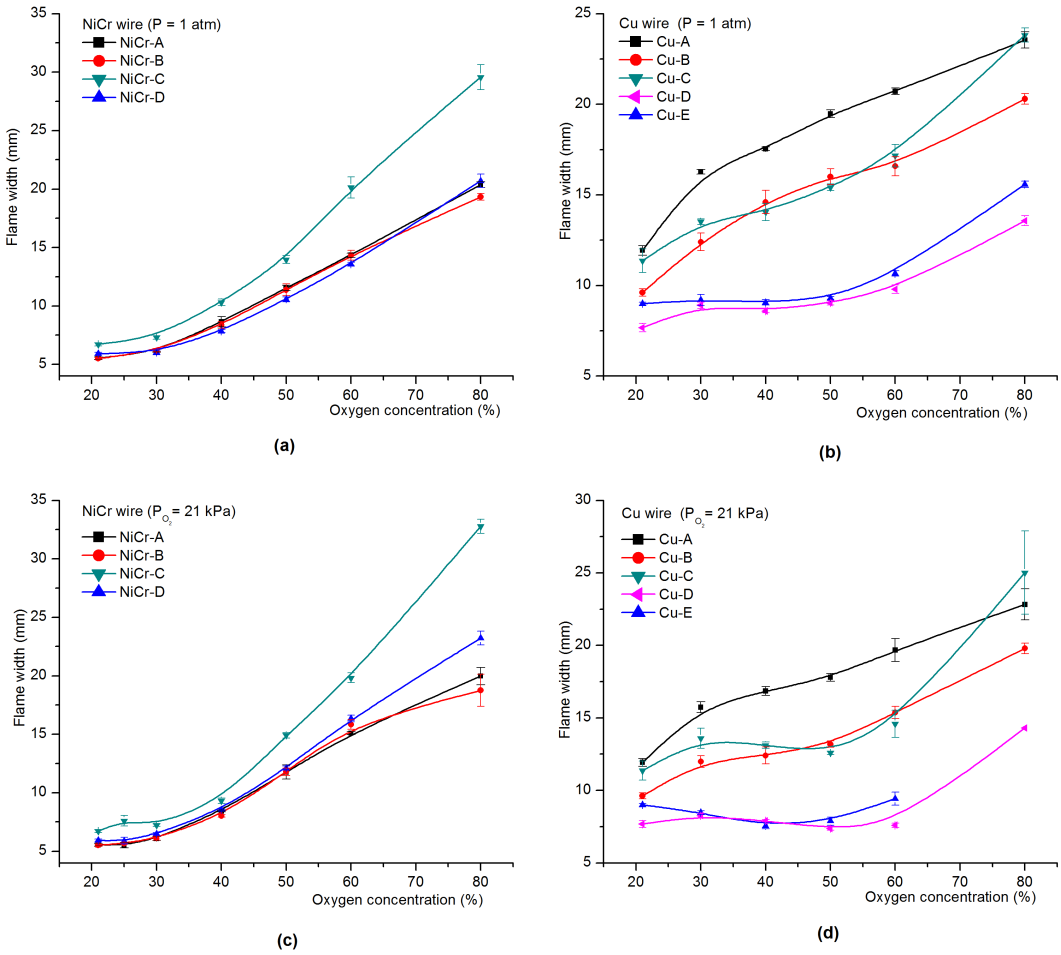

Figure 5.11: Flame widths at different oxygen concentrations: (a) NiCr wires ($P_a = 1$ atm), (b) Cu wires ($P_a = 1$ atm), (c) NiCr wires ($P_{O_2} = 21$ kPa), and (d) Cu wires ($P_{O_2} = 21$ kPa).

Cu-B to Cu-D wires which have the same outer diameter, flame spreads faster over Cu-B because of a larger core-diameter (conductance). All of these implies that for large-conductivity wires, the diameter of the core (conductance) can affect the spread rate in the same order as wire's outer diameter. More wire sizes and experiments need to be conducted to separate the influence of the wire diameter and core diameter and to make a quantitative analysis in future studies.

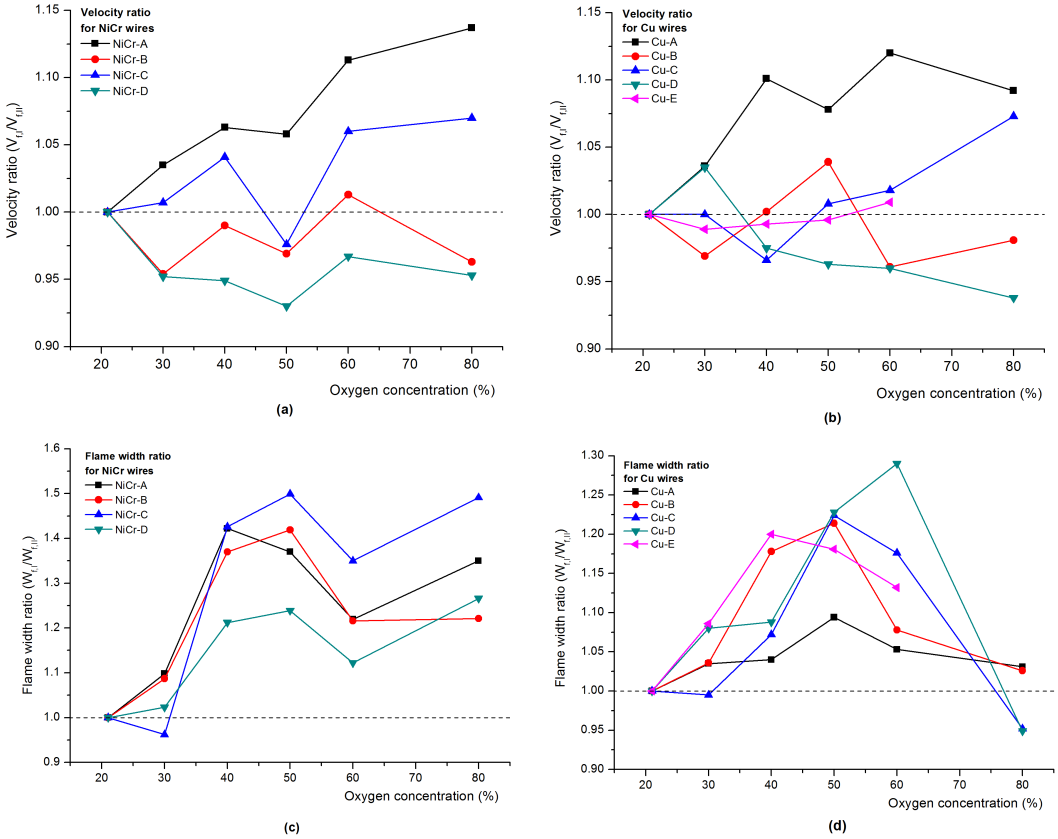

Figure 5.12: Velocity ratios of Test I ($P_a = 1$ atm) to Test II ($P_{O_2} = 21$ kPa): (a) Cu wires; (b) NiCr wires; flame width ratio of Test I ($P = 1$ atm) to II ($P_{O_2} = 21$ kPa): (c) Cu wires; (d) NiCr wires;

5.2.3 Pressure Effect

In order to increase the oxygen concentration at the normoxic pressure ($P_{O_2} = 21$ kPa), the ambient pressure has to be reduced during experiments. Fig. 5.12 shows the ratio of the spread rate and the flame width at $P_a = 1$ atm to those at $P_{O_2} = 21$ kPa. The flame width tends to decrease in reduced-pressure environments (Fig. 5.12c and d), but no clear pattern is discovered for the pressure effect on the spread rate (Fig. 5.12a and b), so there may be two competing pressure effects controlling the spread rate.

As the pressure decreases, the flame becomes weaker, resulting in a lower heat flux in Region II and more frequent dripping than that at the normal at-

mospheric pressure. At the same time, the flame heat flux to Region III (mainly radiation) also changes depending on changes in flame shape, but the convective losses in Region III definitely become small. It is observed in Fig. 5.3 that the glowing bare wire in Region III is more obvious in low-pressure experiments ($P_{O_2} = 21$ kPa), implying a larger net heat flux reaching Region III and resulting a larger spread rate, as shown in Fig. 5.12a. In general, the ambient pressure has a much weaker effect on flame spread, compared to the influence of the modified oxygen concentration. More experiments need be conducted to quantify the pressure effect in the future work.

Table 5.2: Dripping coefficient, ξ during spread over NiCr wires.

X_{O_2}	Set I: $P_a = 1$ atm				Set II: $P_{O_2} = 21$ kPa			
(%)	NiCr-A	NiCr-B	NiCr-C	NiCr-D	NiCr-A	NiCr-B	NiCr-C	NiCr-D
21	0	0	0.30	0	0	0	0.30	0
30	0	0	0.35	0	0	0	0.39	0
40	0	0	0.27	0	0	0	0.39	0
50	0	0	0.17	0	0	0	0.33	0
60	0	0	0	0	0	0	0.15	0
80	0	0	0	0	0	0	0.10	0

Table 5.3: Dripping coefficient, ξ during spread over Cu wires.

X_{O_2}	Set I: $P_a = 1$ atm					Set II: $P_{O_2} = 21$ kPa				
(%)	Cu-A	Cu-B	Cu-C	Cu-D	Cu-E	Cu-A	Cu-B	Cu-C	Cu-D	Cu-E
21	0	0	0.19	0	0.30	0	0	0.19	0	0.30
30	0	0	0.29	0	0.32	0	0	0.41	0.33	0.37
40	0	0	0.27	0.33	0.33	0	0	0.51	0.52	0.59
50	0	0	0.28	0.42	0.45	0	0	0.68	0.70	0.65
60	0	0	0.32	0.40	0.52	0	0	0.81	0.71	0.67
80	0	0	0.32	0.40	0.46	0	0	0.67	0.70	break

5.2.4 Dripping Conditions

For a thick-coated wire, not all the fuel can be burned during the spread process and dripping of the molten ball is observed in experiments for Types C, D and E wires. It is measured that the diameter of the dripping molten ball is about 2 mm for all wires. The dripping coefficients ($0 < \xi = V_b/A_p l_d \leq 1$) are listed in Tables 5.2 for NiCr wires and 5.3 for Cu wires. Here, $\xi = 0$ means no dripping is observed during the whole spread process. Note that in some no-drip cases the molten ball may eventually drip if the wire is long enough, so $\xi = 0$ actually means $\xi < V_b/A_p l_p \approx 0.06$ where l_p is the total length of the coating in the experiment.

Clearly, the dripping coefficient is larger in spread over Cu wires because the lower temperature profile in Region II (Fig. A.2) makes the wire core become a weaker source, as shown in Eq. (2.21). In addition, more frequent dripping is observed in the reduced-pressure experiments because convective heating from the flame decreases due to a weak natural convection effect in low pressures. Since the spread rate changes little with the environmental pressure as discussed above, according to

$$A_b = c_D \bar{P} \rho_c L_p \frac{W_f}{(1-\eta)\dot{q}_f''} \sim \frac{V_f}{(\dot{q}_f'')^2}, \tag{2.22}$$

the required surface area of the molten ball tends to increase as the flame heat flux decreases, becoming easier to exceed a critical value and eventually drop.

As the oxygen concentration increases, the dripping frequency for NiCr-C wire first increases ($X_{O_2} \leq 30\%$), then decreases ($X_{O_2} > 30\%$). Note that as shown in Fig. 5.11a and c, the flame width changes only slightly at $X_{O_2} \leq 30\%$ while the flame heat flux increases appreciably. According to Eq. (2.22), this should lead to less frequent dripping, contrary to experimental observation. It is possible that the viscosity decreases rapidly as oxygen concentration increases, resulting in a large c_D and small critical size of the molten ball. Once $X_{O_2} > 30\%$, the flame width and the spread rate increase faster than the flame heat flux, decreasing the dripping frequency.

For Cu-C/D/E wires, the dripping coefficient decreases as the oxygen concentration increases upon $X_{O_2} = 60\%$ because the flame width changes very little, as shown in Fig. 5.11b and d. Once $X_{O_2} > 60\%$, dripping frequency decreases

because of a large increase in the flame width. The dripping of the polymer during spread is a very complicated problem, and more research on this topic is desired.

Chapter 6

Conclusions

In this study, a simplified ignition-to-spread model was developed to describe the initiation of electrical wire fires by external heat flux. The model predicts that after ignition, the weak flame may be quenched during the transition to flame spread. For a higher-conductance wire, the model predicts that it is more difficult to achieve ignition and that a greater amount of heat is required to sustain the flame in this transition, both of which predictions are confirmed through experimental study with several sample wires. In addition, an increasing heating length facilitates the ignition and makes the spread point converge to the flashpoint, according to both the model and the experiment. The influence of environmental pressure on wire ignition is small compared to influences of modifications in the convective heating sources. Oxygen enrichment strongly promotes the development of spread, but, if excessive, may degrade the model.

Then, a simplified model of horizontal flame spread over thin electrical wires is developed to understand how the wire configuration, thermal conductivity of the wire core, and oxygen concentration affect the spread rate under different ambient conditions. Two sets of experiments under different oxygen concentrations on several thin Cu and NiCr wires were performed, the results of which qualitatively agree with model predictions. As the oxygen concentration increases, the flame-spread rate increases significantly. The thermal conductivity of the wire core plays an important role with the spread rate, which could be on the same order as the effect of wire dimension. In general, for a wire with a smaller diameter

and larger conductance (larger wire core and thermal conductivity), the flame will spread faster, implying more fire-hazardous and contrary to being more difficult to ignite. In addition, comparison of two sets of experiments indicates that the influence of ambient pressure on wire spread is small, compared to the large influence of ambient oxygen concentration. During flame spread, dripping of the molten polymer is observed for thicker-coated wires. More frequent dripping occurs over larger-conductivity wires and at lower pressures.

The proposed model may be useful in the selection and design of fire-safe wires. Future research is desired to (1) find the critical/minimum coating thickness for flame spread; (2) measure the temperature profile during flame spread as well as testing more wires with different metal cores and dimensions to optimize the spread model; (3) investigate the development and hazards of molten drops of burning fuels; and (4) evaluate the applicability of the theory to other more widely used wires.

Appendix A

Derivations of the Wire-Core Temperature Profile

The governing heat-transfer equation of the wire core is

$$A_c\lambda_c\frac{d^2T}{dx^2}+\left(\rho_c c_c A_c\right)V_f\frac{dT}{dx}=\dot{q}_R^{'}. \tag{2.4}$$

In Region I ($x \geq 0$), $\rho_c c_c A_o$ is adopted instead of $\rho_c c_c A_c$, and $\dot{q}_{R,1}^{'} = P_o h_1 (T - T_a)$, leading to

$$\begin{aligned} &\left(\frac{\alpha_c A_c}{V_f A_o}\right)\frac{d^2T_1}{dx^2}+\frac{dT_1}{dx}=\frac{P_o h_1}{(\rho_c c_c A_o)V_f}(T_1-T_a), \\ &\text{B.C.s}\quad T(x=0)=T_{ig},\quad \text{and}\quad T(x=\infty)=T_a. \end{aligned} \tag{A.1}$$

The solutions of these equations are

$$\begin{aligned} &T(x)-T_a=(T_{ig}-T_a)e^{r_1 x}, \\ &\frac{dT}{dx}=-r_1(T_{ig}-T_a)e^{r_1 x}<0, \end{aligned} \tag{A.2}$$

$$\begin{aligned} \text{where}\quad r_1 &= -\frac{V_f A_o}{2\alpha_c A_c}\left[1+\sqrt{1+\frac{4P_o h_1 A_c \lambda_c}{(\rho_c c_c A_o V_f)^2}}\right] \\ &\approx -\frac{V_f A_o}{\alpha_c A_c}\left[1+\frac{(\lambda_c A_c)}{V_f^2}\frac{P_o h_1}{(\rho_c c_c A_o)^2}\right]<0. \end{aligned} \tag{A.3}$$

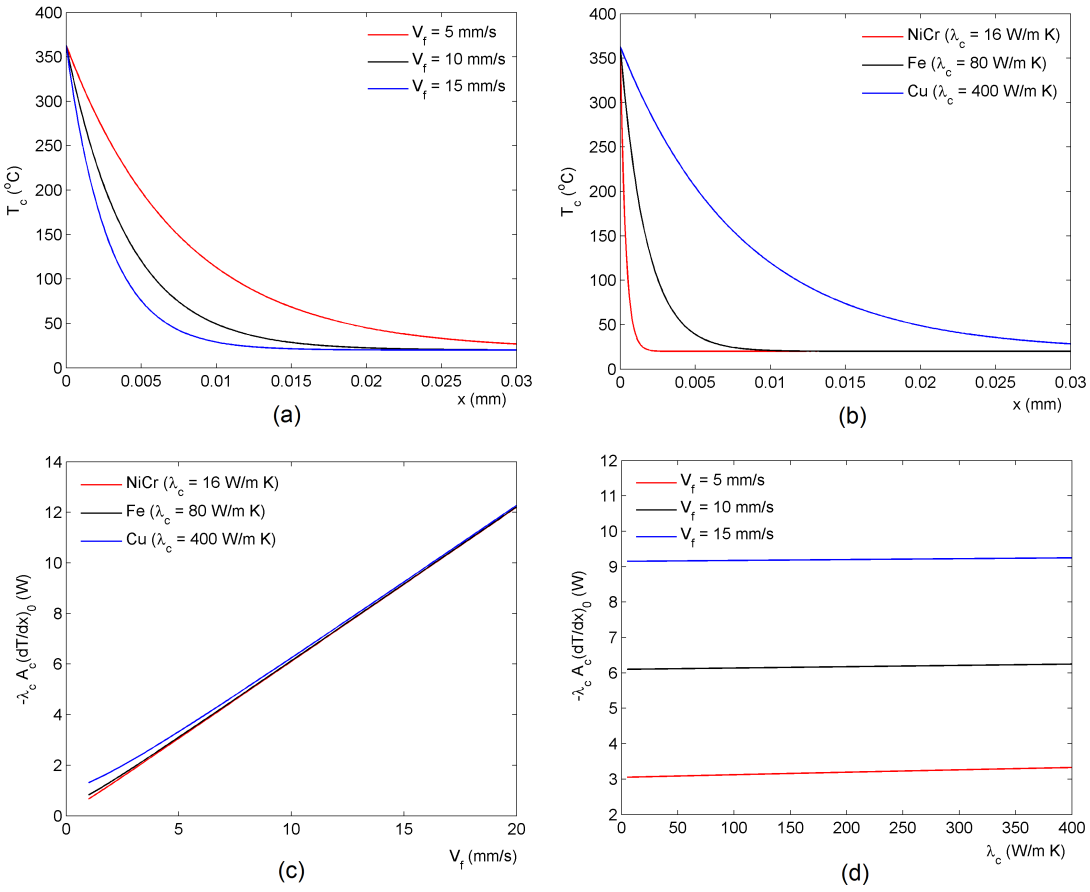

Figure A.1: In Region I, for B-Type wires (a) the temperature profile for different spread rates (Cu-B), (b) the temperature profile for different conductivities ($V_f = 5$ mm/s), (c) conduction from Region II to I for different spread rates, and (d) conduction from Region II to I for different conductivities.

Therefore, conduction from Region II to I is

$$\begin{aligned} -A_c\lambda_c\left(\frac{dT}{dx}\right)_{0^+} &= (\rho_c c_c A_o)\frac{V_f}{2}\left[1+\sqrt{1+\frac{(\lambda_c A_c)}{V_f^2}\frac{P_o h_1}{(\rho_c c_c A_o)^2}}\right](T_{ig}-T_a) \\ &\approx (\rho_c c_c A_o)V_f\left[1+\frac{(\lambda_c A_c)}{V_f^2}\frac{P_o h_1}{(\rho_c c_c A_o)^2}\right](T_{ig}-T_a). \end{aligned} \tag{A.4}$$

Fig. A.1 shows how the temperature profile and conduction from Region II to I change with different spread rates and thermal conductivities. The temperature profile is very sensitive to both the conductivity and the spread rate (Fig. A.1a and b). However, conduction along the wire core increases almost linearly with the

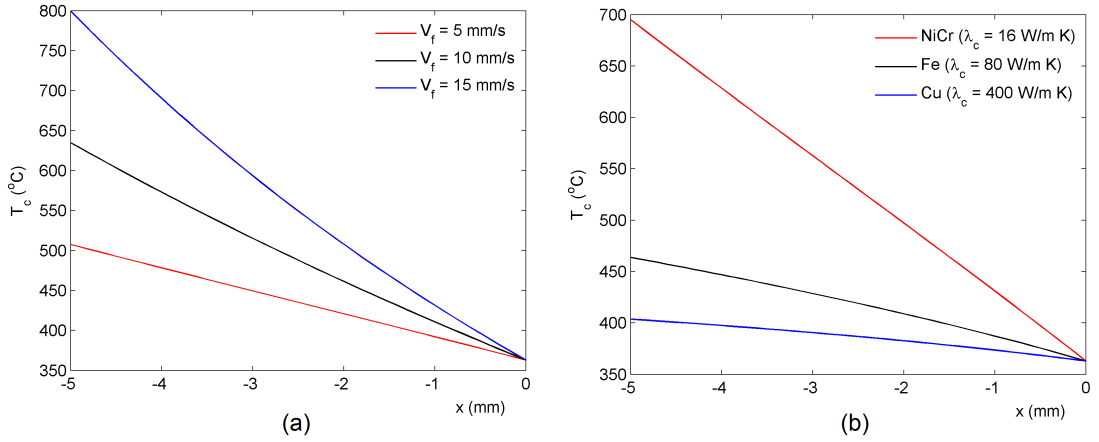

Figure A.2: The temperature profile in Region II, (a) for different spread rates (Cu-B wire), (b) for different conductivities ($V_f = 2$ mm/s, B-Type wire).

spread rate and varies little with the thermal conductivity (Fig. A.1c and d). In other words, the first term in Eq. (A.3) is dominant and the second term is small enough to be neglected, especially when the spread rate is large.

In Region II ($-W_f \leq x < 0$), with $\dot{q}'_{R,2} = P_c[h_b(T-T_{ig})-\eta\dot{q}''_f]$, Eq. (2.4) becomes

$$\left(\frac{\alpha_c}{V_f}\right)\frac{d^2T}{dx^2} + \frac{dT}{dx} = \frac{P_c\left[h_b(T-T_{ig})-\eta\dot{q}''_f\right]}{(\rho_c c_c A_c)V_f},$$
$$\text{B.C.s} \quad T(x=0) = T_{ig}, \quad \text{and} \quad \left(\frac{dT}{dx}\right)_{0^-} = \left(\frac{dT}{dx}\right)_{0^+}. \tag{A.5}$$

The solution is

$$T(x) - T_{ig} = \frac{e^{r_{21}x} - e^{r_{22}x}}{r_{21}-r_{22}}\left[\left(\frac{dT_2}{dx}\right)_{0^-} + \frac{\eta\dot{q}''_f r_{22}}{h_b}\right] + \frac{\eta\dot{q}''_f}{h_b}\left(1-e^{r_{22}x}\right),$$
$$\text{where} \quad r_{21} = \frac{V_f}{2\alpha_c}\left[-1+\sqrt{1+\frac{4P_c h_b \alpha_c}{\rho_c c_c A_c V_f}}\right] > 0 \tag{A.6}$$
$$r_{22} = \frac{V_f}{2\alpha_c}\left[-1-\sqrt{1+\frac{4P_c h_b \alpha_c}{\rho_c c_c A_c V_f}}\right] < 0$$

Therefore, the temperature change in Region II ($T_{-W_f} - T_{ig}$) is

$$\Delta T_2 = \frac{e^{-r_{21}W_f} - e^{-r_{22}W_f}}{r_{21}-r_{22}}\left[\left(\frac{dT_2}{dx}\right)_{0^-} + \frac{\eta\dot{q}''_f r_{22}}{h_b}\right] + \frac{\eta\dot{q}''_f}{h_b}\left(1-e^{-r_{22}W_f}\right), \tag{A.7}$$

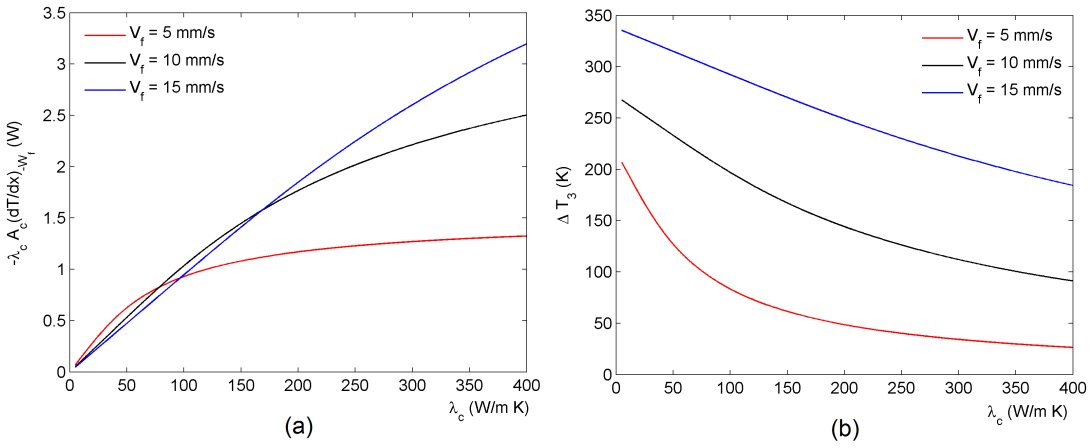

Figure A.3: (a) conduction from Region III to II for different conductivities and spread rates (B-Type wire), and (b) the temperature change in Region III (ΔT_3) for different conductivities and spread rates (B-Type wire).

which is smaller at a larger spread rate (Fig. A.2a) and for a larger-conductance wire (Fig. A.2b). Note that in reality, neither the boiling heat transfer coefficient nor the heat flux from the flame is uniform in Region II, both of which change with the core temperature and the thickness of the coating. But qualitatively, the trend should agree with the simplified model, as discussed above.

In Region III ($-x_m \leq x < -W_f$), the net heat flux to the wire core, $\dot{q}'_{R,3} = P_c \dot{q}''_{f,net} = P_c[\dot{q}''_f e^{(x+W_f)/W_f} - \sigma(T(x)^4 - T_a^4)]$ is assumed to be a constant, yielding

$$\begin{gathered} \left(\frac{\alpha_c}{V_f}\right)\frac{d^2T}{dx^2} + \frac{dT}{dx} = -\frac{P_c \dot{q}''_{f,net}}{(\rho_c c_c A_c)V_f}, \\ \text{B.C.s} \quad T(x=-x_m) = T_{max}, \quad \text{and} \quad \left(\frac{dT}{dx}\right)_{-x_m} = 0. \end{gathered} \tag{A.8}$$

The solutions are

$$\begin{aligned} T(x) &= T_{max} - \frac{P_c \dot{q}''_{f,net}}{(\rho_c c_c A_c)V_f}\left[l_3 - \left(1 - e^{-\frac{(x+x_m)V_f}{\alpha_c}}\right)\frac{\alpha_c}{V_f}\right], \\ \frac{dT}{dx} &= -\frac{P_c \dot{q}''_{f,net}}{(\rho_c c_c A_c)V_f}\left[1 - e^{-(x+x_m)V_f/\alpha_c}\right] < 0. \end{aligned} \tag{A.9}$$

Therefore, conduction from Region III to II is

$$-A_c\lambda_c\left(\frac{dT}{dx}\right)_{-W_f} = \frac{\alpha_c P_c \dot{q}''_{f,net}}{V_f}\left(1 - e^{-l_3 V_f/\alpha_c}\right), \tag{A.10}$$

which is larger for a larger-conductivity wire (Fig. A.3a). If $l_3 V_f/\alpha_c < 1$, $e^{-l_3 V_f/\alpha_c} \approx 1 - l_3 V_f/\alpha_c + (l_3 V_f/\alpha_c)^2/2$ leads to

$$-A_c\lambda_c \left(\frac{dT}{dx}\right)_{-W_f} \approx P_c l_3 \dot{q}''_{f,net}\left(1 - \frac{V_f l_3}{2\alpha_c}\right). \tag{A.11}$$

If $l_3 V_f/\alpha_c > 1$, $e^{-l_3 V_f/\alpha_c} \to 0$ leads to

$$-A_c\lambda_c \left(\frac{dT}{dx}\right)_{-W_f} = \frac{\alpha_c P_c \dot{q}''_{f,net}}{V_f}. \tag{A.12}$$

Also, the temperature change in Region III ($T_{max} - T_{-W_f}$) is

$$\begin{aligned}\Delta T_3 &= \frac{P_c \dot{q}''_{f,net}}{(\rho_c c_c A_c)V_f}\left[l_3 - \left(1 - e^{-\frac{l_3 V_f}{\alpha_c}}\right)\frac{\alpha_c}{V_f}\right] \\ &\approx \frac{P_c l_3^2 \dot{q}''_{f,net}}{\lambda_c A_c}, \quad (l_3 V_f/\alpha_c < 1) \\ &\approx \frac{P_c \dot{q}''_{f,net}}{(\rho_c c_c A_c)V_f}\left(l_3 - \frac{\alpha_c}{V_f}\right), \quad (l_3 V_f/\alpha_c > 1)\end{aligned} \tag{A.13}$$

which is smaller for a larger-conductivity wire (Fig. A.3b).

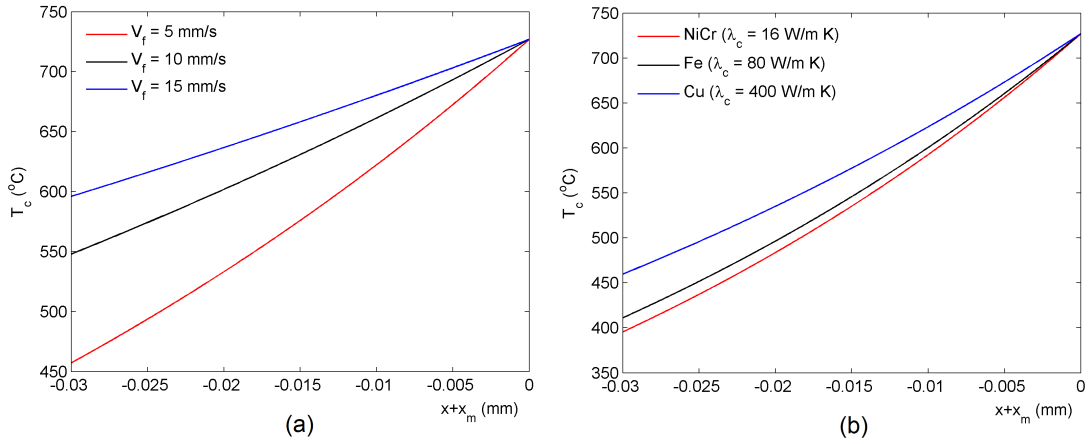

Figure A.4: The temperature profile in Region IV, (a) for different spread rates (Cu-B wire), (b) for different conductivities ($V_f = 5$ mm/s, B-Type wire).

In Region IV ($x < -x_m$), $\dot{q}'_{R,4} = P_o h_4 (T - T_a)$ yields

$$\begin{aligned}\left(\frac{\alpha_c}{V_f}\right)\frac{d^2T_4}{dx^2} + \frac{dT_4}{dx} &= \frac{P_c h_4}{(\rho_c c_c A_c)V_f}(T_4 - T_a), \\ \text{B.C.s} \quad T(x = -x_m) = T_{max}, \quad &\text{and} \quad T(x = -\infty) = T_a.\end{aligned} \tag{A.14}$$

The solutions are

$$\begin{aligned} T(x) - T_a &= (T_{max} - T_a)e^{r_4(x+x_m)}, \\ \frac{dT}{dx} &= r_4(T_{max} - T_a)e^{r_4(x+x_m)} > 0, \end{aligned} \tag{A.15}$$

$$\text{where} \quad r_4 = \frac{V_f}{2\alpha_c}\left[-1 + \sqrt{1 + \frac{4P_c h_4 A_c \lambda_c}{(\rho_c c_c A_o V_f)^2}}\right] \approx \frac{P_c h_4}{(\rho_c c_c A_c)V_f} > 0. \tag{A.16}$$

Fig. A.4 shows how the temperature profile in Region IV changes with different spread rates and thermal conductivities. The temperature decreases faster for a lower conductivity wire, but decreases faster at a lower spread rate, contrary to that in Region I (Fig. A.1a). Comparatively, the conductivity effect is smaller, which supports the approximation in Eq. (A.16).

Control Volume: taking Region II as the control volume, integrating Eq. (A.5) over it yields

$$\begin{aligned} &A_c\lambda_c\left[\left(\frac{dT}{dx}\right)_0 - \left(\frac{dT}{dx}\right)_{-W_f}\right] + (\rho_c c_c A_c)V_f(-\Delta T_2) \\ &= \int_{-W_f}^{0} P_c[h_b(T_2 - T_{ig}) - \eta\dot{q}_f^{''}]dx \approx P_c W_f(h_b\frac{\Delta T_2}{2} - \eta\dot{q}_f^{''}). \end{aligned} \tag{A.17}$$

If the heat flux from the flame is much larger than the boiling heat transfer in Region II ($\dot{q}_f^{''} \gg h_b\Delta T$), substituting the flame width from Eq. (2.16) leads to

$$RHS = -\frac{(P_c\rho_p\delta_p L_p)V_f(\eta\dot{q}_f^{''} - h_b\Delta T_2/2)}{(1-\eta)\dot{q}_f^{''} + h_b\Delta T_2/2 + c_D\rho_p L_p} \approx -\frac{\eta}{1-\eta}(P_c\rho_p\delta_p L_p)V_f. \tag{A.18}$$

If $l_3 V_f/\alpha_c < 1$, substituting Eq. (A.3) and Eq. (A.11) shows

$$\begin{aligned} &P_c l_3\dot{q}_{f,net}^{''}\left(1 - \frac{V_f l_3}{2\alpha_c}\right) - (\rho_c c_c A_o)V_f\left[1 + \frac{(\lambda_c A_c)}{V_f^2}\frac{P_o h_1}{(\rho_c c_c A_o)^2}\right](T_{ig} - T_a) \\ &= -\frac{\eta}{1-\eta}(P_c\rho_p\delta_p L_p)V_f + (\rho_c c_c A_c)V_f\Delta T_2, \end{aligned} \tag{A.19}$$

which is a quadratic equation of V_f

$$\begin{aligned} &\left[(\rho_c c_c A_o)(T_{ig} - T_a) - \frac{\eta}{1-\eta}(P_c\rho_p\delta_p L_p) + (\rho_c c_c A_c)\Delta T_2 + \frac{P_c l_3^2\dot{q}_{f,net}^{''}}{2\alpha_c}\right]V_f^2 \\ &- \left(P_c l_3\dot{q}_{f,net}^{''}\right)V_f + \frac{(\lambda_c A_c)P_o h_1(T_{ig} - T_a)}{(\rho_c c_c A_o)} = 0. \end{aligned} \tag{A.20}$$

Since the conductivity effect on $-A_c\lambda_c\left(dT/dx\right)_0$ is small (Fig. A.1c and d), the last constant term in Eq. (A.20) can be neglected, and the spread rate can be solved as

$$V_f \approx \frac{P_c l_3 \dot{q}''_{f,net}}{R + P_c l_3^2 \dot{q}''_{f,net}/2\alpha_c}, \tag{A.21}$$

$$\text{where} \quad R = (\rho_c c_c A_o)(T_{ig} - T_a) - \frac{\eta}{1-\eta}(P_c \rho_p \delta_p L_p) + (\rho_c c_c A_c)\Delta T_2.$$

If $l_3 V_f/\alpha_c > 1$, the spread rate becomes

$$V_f \approx \sqrt{\frac{\alpha P_c l_3 \dot{q}''_{f,net}}{R}}. \tag{A.22}$$

So that the spread rate increases with increasing thermal conductivity.

References

[1] "Electrical fire safety." `http://www.usfa.fema.gov/citizens/home_fire_prev/electrical.shtm`, 2011.

[2] O. Keski-Rahkonen and J. Mangs, "Electrical ignition sources in nuclear power plants: statistical, modelling and experimental studies," *Nuclear Eng. Design*, vol. 213, no. 2-3, pp. 209 – 221, 2002.

[3] R. Friedman, "Fire safety in spacecraft," *Fire Mater.*, vol. 20, no. 5, pp. 235–243, 1996.

[4] N. Aeronautics and S. Administration, "Fire safety in extraterrestrial environments," tech. rep., NASA/TM-1998-207417 (1998).

[5] V. Babrauskas, *Ignition Handbook Database*. Fire Science Publishers, 2003.

[6] F. Jia, M. Patel, E. Galea, A. Grandison, and J. Ewer, "CFD fire simulation of the swiss air flight 111 in-flight fire – part II: Fire spread analysis," *Aeronaut. J*, vol. 110, no. 1107, pp. 303–314, 2007.

[7] M. M. Hirschler, "Survey of fire testing of electrical cables," *Fire Mater.*, vol. 16, no. 3, pp. 107–118, 1992.

[8] A. Fernandez-Pello, H. Hasegawa, K. Staggs, A. Lipska-Quinn, and N. Alvares, "A study of the fire performance of electrical cables," *Fire Safety Sci.*, vol. 3, pp. 237 – 247, 1991.

[9] J. Quintiere, M. Harkleroad, and D. Walton, "Measurement of material flame spread properties," *Combust. Sci. Tech.*, vol. 32, no. 1-4, pp. 67–89, 1983.

[10] C. Leung, J. Staggs, J. Brindley, A. McIntosh, and R. Whiteley, "The effects of an inert central core on the thermal pyrolysis of an electrical cable," *Fire Safety J.*, vol. 34, no. 2, pp. 143 – 168, 2000.

[11] T. Kashiwagi, "Radiative ignition mechanism of solid fuels," *Fire Safety J.*, vol. 3, no. 3, pp. 185 – 200, 1981.

[12] T. Kashiwagi and T. J. Ohlemiller, "A study of oxygen effects on nonflaming transient gasification of PMMA and PE during thermal irradiation," *Proc. Combust. Inst.*, vol. 19, no. 1, pp. 815 – 823, 1982.

[13] T. Kashiwagi, "Polymer combustion and flammability-role of the condensed phase," *Proc. Combust. Inst.*, vol. 25, no. 1, pp. 1423 – 1437, 1994.

[14] A. Umemura, M. Uchida, T. Hirata, and J. Sato, "Physical model analysis of flame spreading along an electrical wire in microgravity," *Proc. Combust. Inst.*, vol. 29, no. 2, pp. 2535 – 2543, 2002.

[15] O. Fujita, T. Kyono, Y. Kido, H. Ito, and Y. Nakamura, "Ignition of electrical wire insulation with short-term excess electric current in microgravity," *Proc. Combust. Inst.*, vol. 33, no. 2, pp. 2617 – 2623, 2011.

[16] "Burning of polymeric coatings on copper wires and glass threads: I. flame propagation velocity," *Combust. Flame*, vol. 41, pp. 17 – 34, 1981.

[17] "Burning of polymeric coatings on copper wires and glass threads: II. critical conditions of burning," *Combust. Flame*, vol. 41, pp. 35 – 43, 1981.

[18] M. A. Delichatsios, R. A. Altenkirch, M. F. Bundy, S. Bhattacharjee, L. Tang, and K. Sacksteder, "Creeping flame spread along fuel cylinders in forced and natural flows and microgravity," *Proceed. Combust. Inst.*, vol. 28, no. 2, pp. 2835 – 2842, 2000.

[19] A. Tewarson and M. Khan, "Flame propagation for polymers in cylindrical configuration and vertical orientation," *Proc. Combust. Inst.*, vol. 22, no. 1, pp. 1231 – 1240, 1989.

[20] P. A. Beaulieu and N. A. Dembsey, "Effect of oxygen on flame heat flux in horizontal and vertical orientations," *Fire Safety J.*, vol. 43, no. 6, pp. 410 – 428, 2008.

[21] M. Kikuchi, O. Fujita, K. Ito, A. Sato, and T. Sakuraya, "Experimental study on flame spread over wire insulation in microgravity," *Proc. Combust. Inst.*, vol. 27, no. 2, pp. 2507 – 2514, 1998.

[22] O. Fujita, M. Kikuchi, K. Ito, and K. Nishizawa, "Effective mechanisms to determine flame spread rate over ethylene-tetrafluoroethylene wire insulation: Discussion on dilution gas effect based on temperature measurements," *Proc. Combust. Inst.*, vol. 28, no. 2, pp. 2905 – 2911, 2000.

[23] Y. Kim, A. Hossain, S. Kim, and Y. Nakamura, "A numerical study on time-dependent melting and deformation processes of phase change material (PCM) induced by localized thermal input," in *Two Phase Flow, Phase Change and Numerical Modeling* (A. Ahsan, ed.).

[24] Y. Nakamura, N. Yoshimura, T. Matsumura, H. Ito, and O. Fujita, "Opposed-wind effect on flame spread of electric wire in sub-atmospheric pressure," *J. Thermal Sci. Tech.*, vol. 3, no. 3, pp. 430–441, 2008.

[25] Y. Nakamura, N. Yoshimura, H. Ito, K. Azumaya, and O. Fujita, "Flame spread over electric wire in sub-atmospheric pressure," *Proc. Combust. Inst.*, vol. 32, no. 2, pp. 2559 – 2566, 2009.

[26] Y. Nakamura, K. Azumaya, N. Yoshimura, H. Ito, and O. Fujita, "Ignition and subsequent flame spread of polymer-coated wires in sub-atmospheric pressure," 9th International Symposium on Fire Safety Science, (Karlsruhe, Germany), September 2008.

[27] D. Drysdale, *An Introduction to Fire Dynamics, 3rd Ed.* John Wiley and Sons, New York, 2011.

[28] J. G. Quintiere, *Fundamentals of Fire Phenomena*. John Wiley and Sons, New York, 2006.

[29] "Burning rate of fuel cylinders," *Combust. Flame*, vol. 32, pp. 271 – 276, 1978.

[30] J. L. Torero, T. Vietoris, G. Legros, and P. Joulain, "Estimation of a total mass transfer number from the standoff distance of a spreading flame," *Combust. Sci. Tech.*, vol. 174, no. 11-12, pp. 187–203, 2002.

[31] A. Liñán and V. N. Kurdyumov, "Laminar free convection induced by a line heat source, and heat transfer from wires at small grashof numbers," *J. Fluid Mech.*, vol. 362, pp. 199–227, 1998.

[32] F. A. Williams, "Mechanisms of fire spread," *Proc. Combust. Inst.*, vol. 16, no. 1, pp. 1281 – 1294, 1977.

[33] A. Fernandez-Pello, "The solid phase," in *Combustion Fundamentals of Fire* (G. Cox, ed.), ch. 2, pp. 31–100, San Diego, CA: Academic Press INC., 1995.

[34] Y. Nakamura and J. Iwakami, *Personal communication*.

[35] F. Incropera and D. DeWitt, *Fundamentals of Heat and Mass Transfer*. John Wiley & Sons, 2007.

[36] M. A. Delichatsios, "Creeping flame spread: Energy balance and application to practical materials," *Proceed. Combust. Inst.*, vol. 26, no. 1, pp. 1495 – 1503, 1996.

[37] J. E. Parrott and A. D. Stuckes, *Thermal Conductivity of Solids*. Pion, London, 1975.

[38] X. Huang, Y. Nakamura, and F. A. Williams, "Ignition-to-spread transition of externally heated electrical wire," Proc. Combust. Inst. (accepted), 2012.

[39] X. Huang, Y. Nakamura, and F. A. Williams, "An experimental study on ignition of electrical wire," Western States Section of the Combustion Institute, Fall Technical Meeting, (Riverside, CA), Octorber 2011.

[40] D. Drysdale and H. Thomson, "Flammability of plastics II: Critical mass flux at the firepoint," *Fire Safety J.*, vol. 14, no. 3, pp. 179 – 188, 1989.

[41] J. Brandrup, E. H. Immergut, E. A. Grulke, A. Abe, and D. R. Bloch in *Polymer Handbook, 4th Ed.*, John Wiley & Sons, 2005.